NBS TECHNICAL NOTE 607

The Errors in Plasma Measurements by the Microwave Cavity Techniques

NATIONAL BUREAU OF STANDARDS

The National Bureau of Standards[1] was established by an act of Congress March 3, 1901. The Bureau's overall goal is to strengthen and advance the Nation's science and technology and facilitate their effective application for public benefit. To this end, the Bureau conducts research and provides: (1) a basis for the Nation's physical measurement system, (2) scientific and technological services for industry and government, (3) a technical basis for equity in trade, and (4) technical services to promote public safety. The Bureau consists of the Institute for Basic Standards, the Institute for Materials Research, the Institute for Applied Technology, the Center for Computer Sciences and Technology, and the Office for Information Programs.

THE INSTITUTE FOR BASIC STANDARDS provides the central basis within the United States of a complete and consistent system of physical measurement; coordinates that system with measurement systems of other nations; and furnishes essential services leading to accurate and uniform physical measurements throughout the Nation's scientific community, industry, and commerce. The Institute consists of a Center for Radiation Research, an Office of Measurement Services and the following divisions:

Applied Mathematics—Electricity—Heat—Mechanics—Optical Physics—Linac Radiation[2]—Nuclear Radiation[2]—Applied Radiation[2]—Quantum Electronics[3]—Electromagnetics[3]—Time and Frequency[3]—Laboratory Astrophysics[3]—Cryogenics[3].

THE INSTITUTE FOR MATERIALS RESEARCH conducts materials research leading to improved methods of measurement, standards, and data on the properties of well-characterized materials needed by industry, commerce, educational institutions, and Government; provides advisory and research services to other Government agencies; and develops, produces, and distributes standard reference materials. The Institute consists of the Office of Standard Reference Materials and the following divisions:

Analytical Chemistry—Polymers—Metallurgy—Inorganic Materials—Reactor Radiation—Physical Chemistry.

THE INSTITUTE FOR APPLIED TECHNOLOGY provides technical services to promote the use of available technology and to facilitate technological innovation in industry and Government; cooperates with public and private organizations leading to the development of technological standards (including mandatory safety standards), codes and methods of test; and provides technical advice and services to Government agencies upon request. The Institute also monitors NBS engineering standards activities and provides liaison between NBS and national and international engineering standards bodies. The Institute consists of the following technical divisions and offices:

Engineering Standards Services—Weights and Measures—Flammable Fabrics—Invention and Innovation—Vehicle Systems Research—Product Evaluation Technology—Building Research—Electronic Technology—Technical Analysis—Measurement Engineering.

THE CENTER FOR COMPUTER SCIENCES AND TECHNOLOGY conducts research and provides technical services designed to aid Government agencies in improving cost effectiveness in the conduct of their programs through the selection, acquisition, and effective utilization of automatic data processing equipment; and serves as the principal focus within the executive branch for the development of Federal standards for automatic data processing equipment, techniques, and computer languages. The Center consists of the following offices and divisions:

Information Processing Standards—Computer Information—Computer Services—Systems Development—Information Processing Technology.

THE OFFICE FOR INFORMATION PROGRAMS promotes optimum dissemination and accessibility of scientific information generated within NBS and other agencies of the Federal Government; promotes the development of the National Standard Reference Data System and a system of information analysis centers dealing with the broader aspects of the National Measurement System; provides appropriate services to ensure that the NBS staff has optimum accessibility to the scientific information of the world, and directs the public information activities of the Bureau. The Office consists of the following organizational units:

Office of Standard Reference Data—Office of Technical Information and Publications—Library—Office of Public Information—Office of International Relations.

---

[1] Headquarters and Laboratories at Gaithersburg, Maryland, unless otherwise noted; mailing address Washington, D.C. 20234.
[2] Part of the Center for Radiation Research.
[3] Located at Boulder, Colorado 80302.

UNITED STATES DEPARTMENT OF COMMERCE
Maurice H. Stans, Secretary
U.S. NATIONAL BUREAU OF STANDARDS • Lewis M. Branscomb, Director

NBS TECHNICAL NOTE 607

ISSUED OCTOBER 1971

Nat. Bur. Stand. (U.S.), Tech. Note 607, 64 pages (Oct. 1971)
CODEN: NBTNA

The Errors in Plasma Measurements by the Microwave Cavity Techniques

K-B Persson and E. G. Johnson, Jr.

Quantum Electronics Division
Institute for Basic Standards
National Bureau of Standards
Boulder, Colorado 80302

NBS Technical Notes are designed to supplement the Bureau's regular publications program. They provide a means for making available scientific data that are of transient or limited interest. Technical Notes may be listed or referred to in the open literature.

This research was supported in part by the Advanced Research Projects Agency under ARPA Order 703.

For sale by the Superintendent of Documents, U.S. Government Printing Office, Washington, D.C. 20402
(Order by SD Catalog No. C13.46:607), Price 65 cents

Contents

List of Figures

The Errors in Plasma Measurements by the Microwave Cavity Techniques

K-B Persson and E. G. Johnson

This report presents the results of a theoretical and experimental study of the microwave cavity techniques used in measuring electron density and collision frequency in transient plasmas. Sources of errors are discussed and certain calibration procedures are recommended to minimize the error. In particular, the abnormal negative glow discharge in helium is presented as an inexpensive reference plasma for calibration purposes.

Key words: Collision frequency; helium negative glow discharge; microwave cavity; plasma density.

1. Introduction

The purpose of this study is to determine and evaluate the assumptions involved in using the microwave cavity technique to measure the electron density and electron collision frequency for an otherwise unknown plasma, and to make recommendations which will improve the present procedures. The paper is divided into four different sections. A final section contains six appendices which show the mathematical and experimental details.

2. Classes of Plasma Measurement Procedures

The ballistic ranges are interested in measurement of the properties of the plasma generated in the wake of supersonic projectiles.[1-6] The electron density range in these wakes varies from 10^{11} cm^{-3} to less than 10^{5} cm^{-3}. The relaxation times of the plasmas are in the range of tens to hundreds of msec. The electron density range is too large to be subjected to measurements with only one method; hence the range is covered by using several different, but overlapping methods. The ballistic ranges use the following microwave methods:

1. The microwave interferometer.
2. The open microwave cavity (Fabry-Perot).
3. The closed microwave cavity.

The microwave interferometer measures the electron density in the upper end of the range. The closed microwave cavity measures the electron density in the lower end of the range. Several open microwave cavities, operated at different resonance frequencies cover the range between the microwave interferometer and the closed microwave cavity. The measurements in the ballistic ranges are one-shot experiments, that is, all the measurements must be accomplished within times corresponding to the relaxation time of the wake plasma. Economical-technical reasons then favor measuring techniques based on amplitude and phase angle measurements at fixed frequencies.

The microwave interferometer can, if properly used, be labelled as a basic and reliable method and hence can be incorporated in a calibration scheme. However, it can be used reliably only in the high electron density end of the range.

The open microwave cavity has, in addition to properties associated with the closed cavity, problems related to diffraction losses. This study primarily directs itself toward understanding the closed cavity system. When appropriate, the description of the closed cavity system also applies to the open system. The closed cavity system is used with two different measurement procedures: (a) the frequency shift method and (b) the phase and amplitude method. Both these methods give a collision frequency, ν_m, and an average electron density $\langle n \rangle_{aa}$.

The simplest and most reliable is the frequency shift method, where all measurements are done at the resonance radian frequency, ω of the cavity-plasma system. It is shown in Appendix A that in the perturbation range, where one finds a linear relation between the changes in the resonance characteristics and the plasma parameter, that the shift $\Delta\omega$ of the cavity due to the insertion of the plasma, is related to the average electron density, defined in A-14, as follows:

$$\langle n \rangle_{aa} = \frac{2m\varepsilon_o}{e^2} \left(\omega^2 + \nu_m^2 \right) \frac{\Delta\omega}{\omega} \quad . \tag{1}$$

To obtain the momentum transfer collision frequency it is in addition necessary to measure the attenuation of the signal transmitted through the cavity. The electron momentum transfer collision frequency ν_m is then determined by the formula

$$\nu_m = \left(\frac{S'_o}{S'_p} - 1 \right) \frac{\omega^2}{2Q_L \Delta\omega} \tag{2}$$

where S'_p is the amplitude of the signal, in the presence of the plasma, after it has been transmitted through the cavity while S'_o is the corresponding signal in the absence of the plasma.

The second method, the phase and amplitude method, measures the change in the phase and amplitude, caused by the insertion of the plasma into the cavity, of a signal transmitted through the cavity at a fixed frequency, the resonance frequency of the cavity in the absence of the plasma. The average electron density and the electron collision frequency are then, provided the measurements are done within the perturbation range, obtained from the following formulas

$$\langle n \rangle_{aa} = \frac{m\varepsilon_o}{e^2} \frac{(\omega^2 + \nu_m^2)}{Q_L} \frac{S_o}{S_p} \text{ Sin } (\varphi_p - \varphi_o) \tag{3}$$

and

$$\nu_m = \omega \frac{\text{Cos } (\varphi_p - \varphi_o) - \frac{S_o}{S_p}}{\text{Sin } (\varphi_p - \varphi_o)} \tag{4}$$

where φ_p and S_p are the phase angle and the amplitude of the signal after it has been transmitted through the cavity in the presence of the plasma, while φ_o and S_o are corresponding quantities in the absence of the plasma.

The two methods are contrasted by noting that the frequency shift method relies on a frequency shift and an attenuation measurement. To obtain the same quantity by the phase and amplitude method it is necessary to measure the phase shift, the attenuation, as well as the loaded Q of the system in the absence of the plasma, Q_L. If the two methods are applied to the same cavity-plasma system and there are no errors, the measurements with the two methods are related as follows

$$\frac{\Delta\omega}{\omega} = \frac{1}{2Q_L} \frac{S_o}{S_p} \text{ Sin } (\varphi_p - \varphi_o) \tag{5}$$

and

$$\frac{S'_o}{S'_p} = \frac{S_o}{S_p} \text{ Cos } (\varphi_p - \varphi_o) \tag{6}$$

with the quantities on the left hand side of the equality signs representing measurements by the frequency shift method and the quantities on the right hand side representing measurements by the phase and amplitude method. The fundamental simplicity of the frequency shift method makes it very useful to calibrate other methods provided a reference plasma is available, and the methods are used in the same system. It should be observed that if the same cavity and mode are used for the measurements on the same plasma, as can be the case in the comparison of the frequency shift method and the phase and amplitude method, then they can be compared without interpreting $\langle n \rangle_{aa}$.

3. Sources of Errors in the Cavity Method

Here we look at two classes of errors, the interpretative and the measurement errors. The first are due to simplifications of the theory used to understand the experimental results and the second are due to the experimental paraphernalia and procedures. The first are usually systematic errors and the second may have both systematic and random errors.

3.1 Interpretation errors.

There are two levels of interpretative errors - those involving the cavity mode of interest and those due to other modes.

a. The single mode errors.

The cavity of interest and the cylindrical plasma are shown in figure 1. The cavity has rotational symmetry around the axis A-A. The cylindrical sleeves B are cut-off wave guides attached to the cavity to accommodate plasmas longer than the basic cavity. The idealized version of this cavity, used for the theoretical interpretation of the measurements, is shown in figure 2. The mode with the lowest resonance frequency, the TM_{010} mode, is well separated from the higher modes. The corresponding electric field distribution is shown qualitatively and the analytical form for its electric field distribution is

$$\left.\begin{aligned} E_{az} &= E_o J_o \left(2.405 \frac{r}{R}\right) \\ E_r &= E_\varphi = 0 \ . \end{aligned}\right\} \tag{7}$$

where z is the axial, r the radial, and φ the angular coordinates, while R is the radius and L the length, excluding the sleeves, of the cavity. The real field distribution of the true cavity must, in view of the presence of the sleeves, be written as

$$\left.\begin{aligned} E_{az} &= E_o f\,(r, z; L, R, \zeta, \ell) \\ E_{ar} &= E_o g\,(r, z; L, R, \zeta, \ell) \\ E_y &= 0 \end{aligned}\right\} \tag{8}$$

where f and g are functions of r and z with L, R, ζ, and ℓ as parameters. The radius and length of the sleeves are ζ and ℓ respectively.

Correct average electron density measurements require the use of the real field distribution given by (8) and not the distribution given by (7) as is commonly used. This is particularly important if the measurements with the cavity are compared with measurements done with another cavity with a different field distribution, or with a microwave interferometer. Because the analytical description is not readily available, we suggest that it is better to measure the field distribution by the method described in Appendix B.

In addition to the field distribution error which will produce a systematic error in the electron density we can also have errors traceable to the external circuitry containing the generator, the detecting equipment, and the wave guides or coaxial lines. Usually the cpupling is done so that the resonance characteristics of the mode used for measurements dominate over the frequency characteristics of the external circuits. Two basically different systems are used; the one-port system where one observes the resonance characteristics of the cavity-plasma system on the signal reflected from the cavity and the two-port system where one measures the resonance characteristics on the signal transmitted through the cavity. The two-port system is more sensitive [6] than the one-port system and hence gives a larger range of acceptable measurements. The external circuits do influence the resonance characteristics of the system and may introduce systematic errors in the measurements. Appendix C shows typical errors in a two-port system.

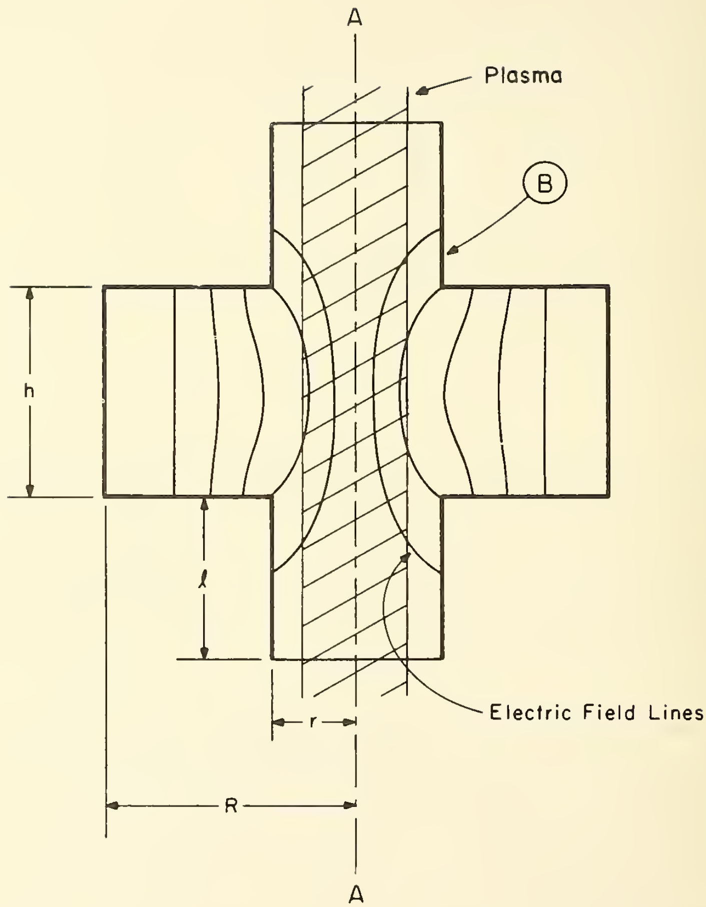

Figure 1. THE STANDARD CAVITY

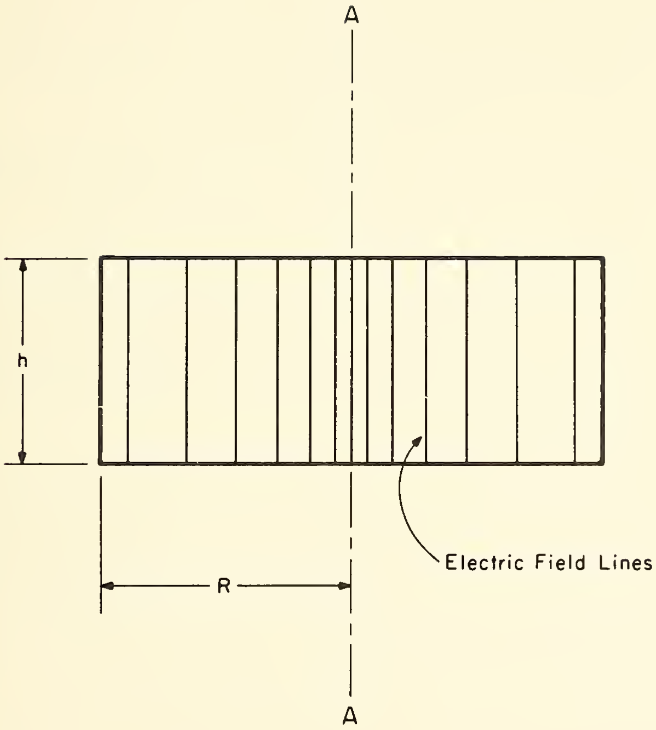

Figure 2. THE IDEAL CAVITY

A final source of systematic errors in the single mode approximation comes from the linearization assumptions of the perturbation theory under high loss conditions. The resonance frequency is experimentally determined as the frequency at which one observes a maximum of the signal transmitted through the cavity. This frequency is influenced not only by the couplings to the external circuits but also by the inherent cavity losses, as well as by the losses in the medium contained by the cavity. Neglecting both the inherent cavity losses, and the influence of the external circuits, one finds from formula (17), Appendix A, that the frequency shift due to the presence of the plasma is a non-linear function of the electron density. The two criteria (18) and (19) of Appendix A determine the upper limits of the linear range. For loss factors less than unity, it is necessary to use the criterion (19) which says that the higher loss factor, the more limited is the linear range.

b. Other mode errors.

We have two classes of additional modes that can be excited because of the nonideal structures in the cavity and the coupling mechanisms, and because of the nonuniformity of the plasma.

(1) Excitation of higher solenoidal modes.

Imperfections in the cavity and the coupling mechanisms (loops and irises) couple to solenoidal modes other than the desired one. These higher modes are suppressed by making the imperfections small and by properly locating and designing the coupling mechanisms. Appendix F shows the experimental effect of different coupling schemes.

When the plasma density approaches the dense condition as is illustrated by formula (27) of Appendix A, we find that the higher modes can be neglected only if the criteria defined by formula (30) and (31) are satisfied. As both these criteria depend on the plasma and the electric field configuration, we see that the linear range is more restricted for the amplitude and phase shift method than for the frequency shift method. This difference can be large depending on the coupling mechanisms. These modes produce systematic frequency and phase shift errors.

(2) Excitation of irrotational modes.

The electric polarization due to the non-uniform plasma or the uniform plasma that partially fills the cavity, and the radial electric fields generate free space charge which in its turn excites irrotational modes. These modes can produce systematic errors in the loss factor measurements in addition to the frequency and phase shift errors. Appendix B shows the strong radial field structure for the cavity system under study. Appendices E and F show the experimental consequences of these fields. Appendix A shows the theoretical consequences.

3.2 Measurement errors.

The measured quantities and the inferred physical parameters are:

<u>The Frequency Shift Method</u>

Physical parameter		Measured quantities
$\dfrac{\langle n\rangle_{aa}}{1+\left(\dfrac{\nu_m}{\omega}\right)^2}$	(modified electron density)	ω_r, ω_o
$\dfrac{\nu_m}{\omega}$		S_o, S_p, ϖ_o, ϖ_p .

The Amplitude and Phase Shift Method

$$\frac{\langle n \rangle_{aa}}{1+\left(\frac{\nu_m}{\omega}\right)^2} \qquad\qquad \omega,\ Q_L,\ S_o,\ S_p,\ \varphi_o,\ \varphi_p$$

$$\frac{\nu_m}{\omega} \qquad\qquad S_o,\ S_p,\ \varphi_o,\ \varphi_p\ . \tag{9}$$

Three types of quantities must be measured, namely: frequencies, phase angles and amplitudes. The determination of Q_L involves frequency and amplitude or phase angle measurements. Because frequencies are measured with high precision, they are henceforth considered error free. The dominant measurement errors are found in the amplitude and phase angle measurements. They depend strongly on the cavity-circuit system, as is demonstrated in Appendix C, and on the measurement electronics, as shown in Appendix F.

The order of accuracy of the inferred physical parameters is as follows. Only the modified average electron density measured with the frequency shift method has no important measurement errors. The loss factor ν_m/ω measured with the same method has measurement errors because it is then necessary to measure two amplitudes and the loaded Q of the system. Because the amplitude and phase shift method determines the loss factor by two phase angles and two amplitude measurements, we expect even less accuracy in this case. The least accurate measurement is the modified average electron density measured by the amplitude and phase shift method. This measurement requires additionally the determination of the system's loaded Q.

The detailed investigation of the frequency shift method in Appendix F shows the validity of the accuracy ordering. The variations in the cavity-circuit system and in the electronics have a definite influence on the amplitude and phase shift measurements and have practically no influence on the modified average electron density as measured by the frequency shift method.

4. Calibration Techniques for the Cavity Method Using the Standard Plasma

Because Appendices A and C show clearly that it is not practical to derive general criteria for each measurement method, which delineate the acceptable linear ranges or proportionality constants, and because there is little hope for any a priori determination of the systematic errors of the total system, we must introduce a bona fide calibration of the system. The calibration requires two things: a reproducible measurement method and a reproducible medium, preferably a plasma, with properties that scan the range of interest and which can be subjected to additional measurements by the methods that can be absolutely calibrated.

The current ballistic range calibration scheme which uses the microwave interferometer as a reference method, can in principle be extended to the low electron density range, where the closed microwave cavity is used for the measurements. However, the cumulative errors in the calibration become very serious because several different instruments must be used to cover the gap in measurements between the interferometer and the closed cavity. This calibration is further complicated because the interferometer and the closed cavity measure different average electron densities. Thus, it is necessary to use a scheme which brings about a closer relation between the microwave cavity measurements and the interferometer measurements.

The standard reference plasma, the pulsed abnormal negative glow in helium of 1 Torr pressure, as described in Appendix D, has all the properties required from a calibration medium, which must be subjected to measurements by both the microwave interferometer and the closed cavity system. Its electron density varies from 10^{12} cm^{-3} in the early afterglow to less than 10^5 cm^{-3} in the very late afterglow. Its relaxation time is of the order 10 msec. The collision frequency of the electrons, $2.6\text{x}10^8$ sec^{-1}, is sufficiently small so the presence of the loss factor can be neglected in the measurements with

the closed microwave cavity as well as with the microwave interferometer. The plasma tube is very reproducible in physical construction as well as in terms of the measurement results during its operating life time. It can also be manufactured in sizes commensurate with the wake plasmas. Because it can be operated in the repetitive pulse mode, or in single shot mode, as is done in the ballistic ranges, it is amenable to reliable reference methods for the calibration.

Because the microwave interferometer and the closed microwave cavity do not measure the same spatial averages of the electron density, it is necessary to know accurately the electric field distribution of the cavity and the spatial distribution of the plasma. As this is not true for the given cavity system, we need a reference method which does not require precise knowledge of the spatial electron density. As already shown, the frequency shift method is such a method. The interpretation of the measured average electron density is then deferred until the measurements are compared with the microwave interferometer measurements.

5. Examples of Errors in Different Ballistic Ranges

The investigation of the frequency shift method for measuring the average electron density of the standard reference plasma (see Appendix F) shows that this method is remarkably insensitive to variations in the circuitry and the electronics. It is therefore a good reference method for the cavity measurements. It becomes sensitive to the circuitry and the electronics only for the loss factor measurements because then it is necessary to use amplitude and loaded Q measurements. This experience implies that any method based on amplitude and phase shift measurements could be subject to large errors. Since all measurements at the ballistic ranges are based on amplitude and phase angle measurements, a direct comparison using the standard reference tube and the equipment necessary for the frequency shift measurements was made at two of the ballistic ranges.

5.1 Two-port cavity method

The first visit was at the Lincoln Laboratories, Mass., where, with the cooperation of Dr. W. M. Kornegay, a series of comparative measurements were made with the standard reference plasma inserted in one of the range cavities. Dr. Kornegay used the amplitude and phase shift method on a two-port [1,2] system with the measuring technique developed by Lincoln Laboratories. NBS used the frequency shift method as developed at NBS, Boulder. A typical result of these comparative measurements is shown in figure 3, where the frequency shift due to the presence of the plasma has been plotted as function of the time in the afterglow of the standard reference plasma. The fully drawn curve represents the NBS measurements. The crosses and circles represent data point derived from single shot runs taken by Lincoln Laboratories with the amplitude and phase shift method. Their amplitude and phase shift measurements have been converted into an equivalent frequency shift with the help of formula (5) in order to be comparable with the NBS measurements. The discrepancy between the measurements is large; the amplitude and phase shift method measures the electron density almost an order magnitude smaller than the frequency shift method. The two curves are almost parallel; indicating that the system used by Lincoln Laboratories is linear, but with a proportionality constant almost an order of magnitude smaller than predicted by the idealized theory. This error can be corrected through calibration.

5.2 One-port cavity method

The second visit was to ARO, Arnold Air Force Station, Tenn. Here comparative measurements were done with the cooperation of C. P. Enis and again on the standard reference plasma, inserted in one of the range cavities. The method used by ARO was the one-port system with the Smith chart oscilloscope display. [7] NBS used the same frequency shift method as was used at Lincoln Laboratories. The results are shown in figure 4. The data obtained by the one-port system was converted by ARO into an equivalent frequency shift to become comparable with the data obtained by the NBS method. The fully drawn line represents the data obtained by NBS. The crosses and squares represent two sets of data points obtained with the ARO

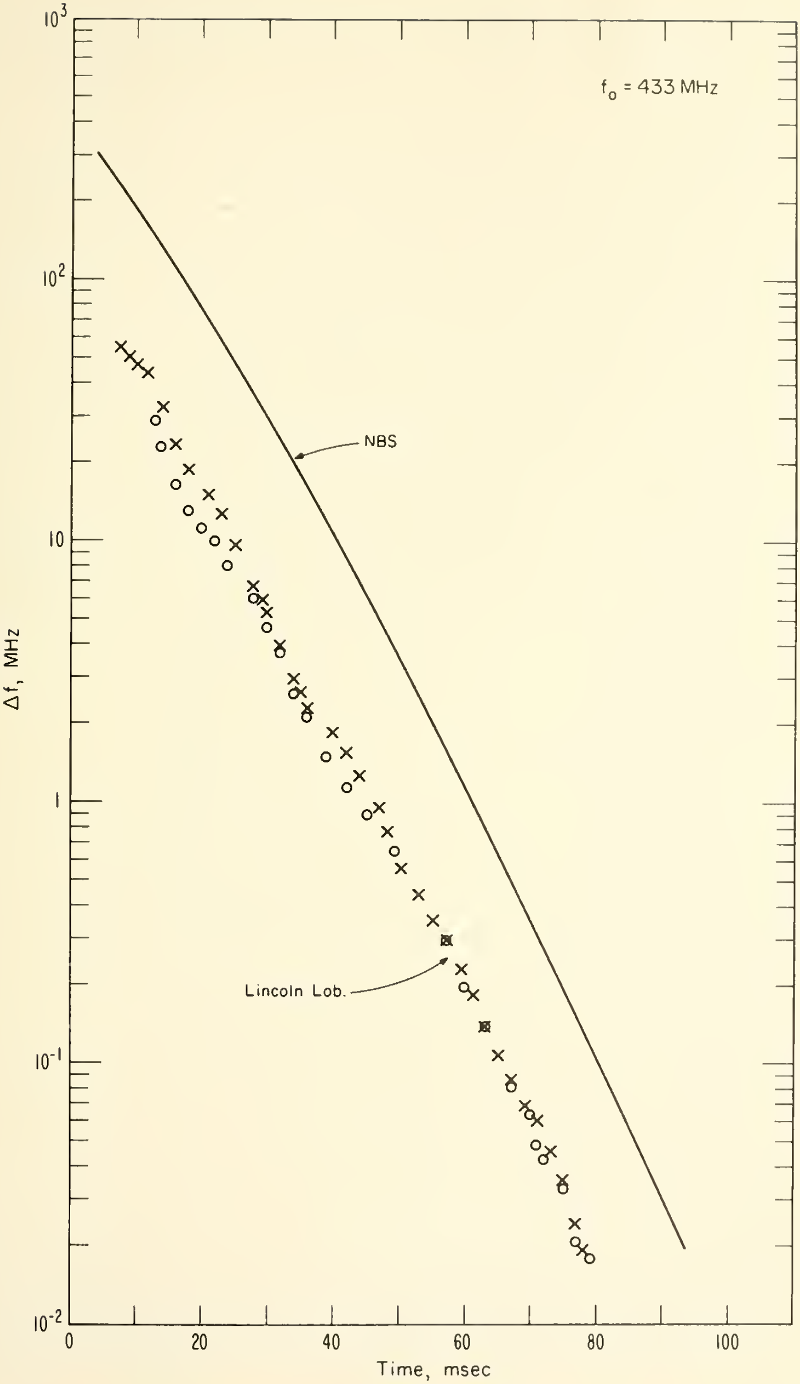

Figure 3. FREQUENCY SHIFT, COMPARISON NBS - LINCOLN LAB.

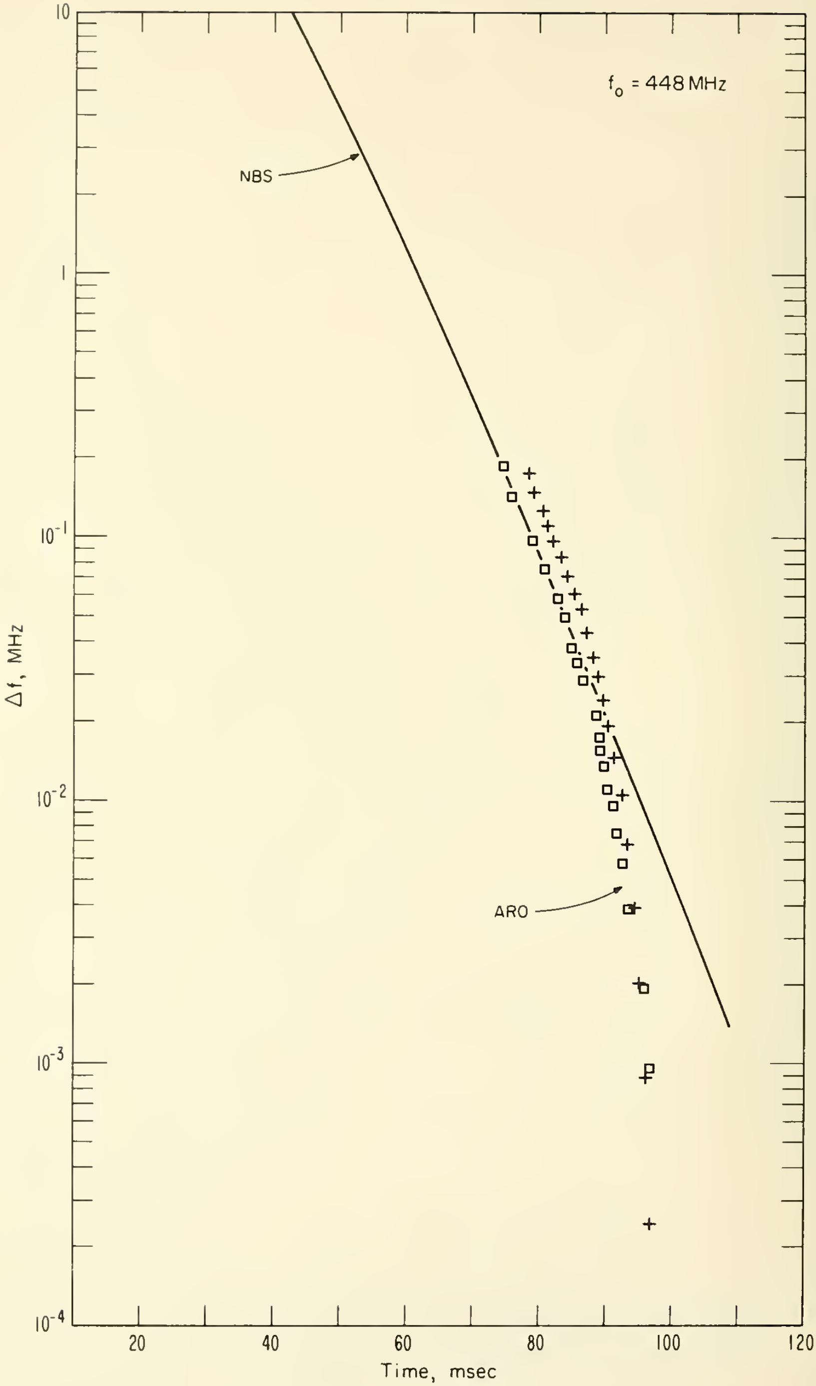

Figure 4. FREQUENCY SHIFT, COMPARISON NBS - ARO

one-port system. We note that the one-port system is much more limited in the dynamic range than the two-port system, and that the one-port system as used by ARO appears to be non-linear. The ARO measurements agree reasonably well with the NBS measurements for high electron densities but are more than an order of magnitude too small at low electron densities. If one accepts only the part of the measurements where the ARO and the NBS measurements agree, then it follows that the one-port system has an acceptable dynamic range of less than an order of magnitude.

D. E. Coffman and C. N. Enis of ARO have made a calibration of the ARO one-port system with the Smith chart oscilloscope display using dry air as a calibrating medium.[7] They demonstrated that they could measure the dielectric constant of dry air under steady state condition, and for a smaller range to within 5 per cent of the value given by NBS. The measurements were done as a function of the air pressure in the range 0 to 500 Torr. Although these measurements must be considered correct, they are not a final calibration relative to the measurements executed in the ballistic ranges, which are done under transient conditions. A dielectric in the form of a gas or solid can not simulate the transient characteristics of the wake plasma. In contrast, the standard reference plasma does simulate the transient characteristics of the wake plasma. This observation suggests that perhaps the major part of discrepancy between the data obtained with methods based on amplitude and phase angle measurements on the one hand and the data obtained from the measurements with the frequency shift methods on the other hand, are traceable to the transient characteristic of the measurement electronics. It is also probable that part of the discrepancy between the Lincoln Laboratories measurements and the NBS measurements has the same source. This is seen because the frequency shift method (see Appendix F) gives no significant errors in the electron density due to the transients in the electronics while the loss measurements are influenced by the transients.

Acknowledgments:

The success of this project has been greatly advanced due to contributions from F. B. Haller in the design and manufacture of the standard plasma tube and from R. Ray in the design of necessary electronic equipment as well as in the execution of the necessary measurements.

6. Conclusions and Recommendations

Because methods based on phase angle and frequency measurements are much less subject to errors caused by transients than are methods involving amplitude measurements we suggest that the microwave interferometer method, which is based on phase angle measurements, and the open or closed cavities, using only frequency shift measurements, should be considered the reference methods. Of these two, the microwave interferometer is the most basic and reliable, but also the least sensitive. The cavity frequency shift method, operated at the same frequency as the interferometer, can be made several orders of magnitude more sensitive. On the other hand, the cavity measurement is less desirable because it measures a more complex average of the electron density. To measure a direct average electron density with either method requires a probing frequency such that the loss factor is negligible relative to unity. If the loss factor is comparable to or larger than unity, as is the case with the wake plasmas, then it becomes necessary to use amplitude measurements which are more prone to errors related to the circuits and the electronics.

To compare above methods to measurements done with more complex ones requires a calibration medium. This medium must have well known properties which scan the total range of interest and also simulate the transient conditions that are characteristic of the wake plasmas. The standard reference plasma described in Appendix D satisfies these requirements. Both reference methods have been used successfully on this plasma under steady state conditions and under the transient situation represented by its afterglow. The comparative measurements done at Lincoln Laboratories and at ARO indicate that the system must be calibrated by a medium simulating the wake transients. Both the Lincoln Laboratories system and the ARO system have been calibrated with dielectrics showing no significant errors. The dielectrics, however, cannot simulate the transient nature of the wake plasma. The discrepancy between the NBS frequency shift method and the amplitude and phase methods used in the ballistic ranges showed up only when the measurements were done on the transient standard reference plasma.

The standard reference plasma is, as yet, not useful in all complex measurement systems available at the ballistic ranges. The open cavity resonator (Fabry-Perot) presents special problems. Preliminary experiments done by R. A. Hayami, AC Laboratories, indicate that the quartz envelope of the standard reference plasma introduces too high diffraction losses when introduced into the open cavity resonator and that it, therefore, cannot be used as a calibration medium for the open cavity resonators, at least not with the presently used measuring techniques.

Both the electric polarization measurements and the measurements of the loss factor show that interpretative errors become apparent when electron density exceeds approximately 1/30 of the critical electron density. The usual average electron density then is inadequate for the interpretation of the measurement. A correct interpretation must include the effects of irrotational modes and higher solenoidal modes. Consequently, the upper limit of the linear range for measuring electron densities with the low frequency (5×10^8 Hz) cavity is about 10^8 cm^{-3} for the standard reference plasma. This is not satisfactory since one must consider that the standard reference plasma has a diameter of 5 inches while the early wake plasma can have a diameter of less than 1 inch. This limits the linear range for the electron density measurements with the low frequency cavity to two or at the most three orders of magnitude.

Because of the inherent limitations of the low frequency, closed cavity method as described above, it is desirable to replace it with some more reliable method. The dispersometer, an instrument used by Liebe, Thompson and Dillon [8, 9] for measuring the dispersivity of gases, seems to have the desired properties. The dispersometer is a double cavity instrument with one cavity serving as a reference cavity. The two cavities, and especially designed electronics, allow frequency shift measurements several orders of magnitude smaller than can be done with conventional methods. Translating the experience

with this instrument into equivalent electron density measurements, one finds that it should be possible to measure the electron density in the plasma, over the range of interest to the ballistic ranges, with one instrument in two modes of operation. This instrument is presently being built by NBS, using two open cavity resonators with the resonance frequencies 35 and 70 GHz. These high frequencies have been chosen to avoid interpretative errors associated with the electric polarization of the wake plasma.

7. References

1. Labitt, M. and Herlin, M., "Application of the Resonant Cavity Method to the Measurement of Electron Densities and Collision Frequencies in the Wakes of Hypervelocity Pellets", Massachusetts Institute of Technology, Lincoln Laboratory Technical Report No. 248, October 1961.
2. Labitt, M., "The Measurement of Electron Density in the Wake of a Hypervelocity Pellet over a Six-Magnitude Range", Massachusetts Institute of Technology, Lincoln Laboratory Technical Report No. 307, April 1963.
3. Primich, R. I. and Hayami, R. A., "The Application of the Focused Fabry-Perot Resonator to Plasma Diagnostics", GM/DRL, TM 63-210, August 1963.
4. Hayami, R. A., et. al., "Fabry-Perot Resonators at 5 Gc and 35 Gc for Wake Ionization Measurements in a Free-Flight Ballistic Range", GM/DRL Report TR 65-19B, May 1965.
5. Hayami, R. A. and Kelley, K. J., "The Measurement of Transient Ionization Levels Using Open Microwave Resonators", GM/DRL Technical Report TR 66-OIK, July 1966.
6. Hendrix, R. E., Radio-Frequency and Microwave Flow-Field Diagnostic Techniques in Aeroballistic Ranges - A Comprehensive Study", AEDC-TR-69-215.
7. Coffman, D. E. and Enis, C. P., "Calibration of a Resonant Cavity System by Measurement of the Dielectric Constant of Air", AEDC-TR-70-11.
8. Thompson, M. C., Jr. and Vetter, M. J., Rev. Sci. Instrum. 38, 1826 (1967).
9. Liebe, H. J., Thompson, M. C., Jr., and Dillon, T. A., J. of Quant. Spectr. and Rad. Transf. 9, 31, (1969).
10. Slater, J. C., "Microwave Electronics", (McGraw-Hill Book Co., Inc., 1950).
11. von Engel, A., "Ionized Gases", (Oxford, The Clarendon Press, 1965).
12. Persson, K. B., J. Appl. Phys. 36, 3086 (1965).
13. Persson, K. B., Phys. Rev. 106, No. 2 (1957).
14. Persson, K. B., Phys. Fluids 5, 1625 (1962).
15. Allis, W. P., "Motion of Ions and Electrons", "Encyclopedia of Physics", Vol. XXI, p. 421, (Springer-Verlag, 1956).
16. Brown, S. C., "Basic Data of Plasma Physics, 1966", p. 17, (The M. I. T. Press, 1967).
17. Panovsky, W. K. H. and Phillips, M., "Classical Electricity and Magnetism", p. 77, (Addison and Wesley, 1955).

The Appendices

Appendix A

A theory for a test body or plasma introduced in a microwave cavity

Any material with finite dielectric constant and/or electric conductivity introduced into an active microwave cavity induces currents and polarization charges which shift the resonance frequencies of the cavity modes. If the cavity is excited at a fixed radian frequency, ω, Maxwell's equations can be written as

$$\begin{aligned} &\vec{\nabla} \times \vec{E} = - j \omega \mu_o \vec{H} \\ &\vec{\nabla} \times \vec{H} = j \omega \varepsilon_o \vec{E} + \vec{J} \\ &\vec{\nabla} \cdot \vec{H} = O \\ &\vec{\nabla} \cdot \vec{E} = g/\varepsilon_o = - \frac{\vec{\nabla} \cdot \vec{J}}{j\omega\varepsilon_o} \end{aligned} \tag{1}$$

where $\vec{J}$, the current density, accounts for all effects of the material introduced into the cavity. The Poynting's equation, integrated over the volume of the cavity, takes the form

$$\langle \vec{E} \times \vec{H}^* \rangle_s = -j\omega \; \mu_o \langle \vec{H} \cdot \vec{H}^* \rangle - \varepsilon_o \langle \vec{E} \cdot \vec{E}^* \rangle \; - \langle \vec{J}^* \cdot \vec{E} \rangle, \tag{2}$$

where $\langle \; \rangle$ implies integration over the volume of the cavity and $\langle \; \rangle_s$ integration over the inside surface of the cavity. To account for the effects of the matter introduced into the cavity, we follow Slater[10] and introduce the solenoidal and irrotational orthonormal modes which satisfy Maxwell's equations and the boundary conditions prescribed by the cavity. The solenoidal set, E_i, H_i and the corresponding resonance frequency ω_i are determined by the equations

$$\begin{aligned} &\vec{\nabla} \times \vec{E}_i = -j\omega_i \mu_o \vec{H}_i \\ &\vec{\nabla} \times \vec{H}_i = j\omega_i E_o \vec{E}_i \\ &\langle \vec{E}_i \times \vec{H}_i^* \rangle_s = O \\ &\mu_o \langle \vec{H}_i \cdot \vec{H}_j^* \rangle = \varepsilon_o \langle \vec{E}_i \cdot \vec{E}_j^* \rangle = \delta_{ij} \end{aligned} \tag{3}$$

while the irrotational set is defined by

$$\begin{aligned} &k_x \vec{F}_s = \vec{\nabla} \Phi_s \\ &\nabla^2 \Phi_s + k_s^2 \Phi_s = O \\ &\langle \vec{n} \times \vec{F}_s \rangle_S = O \\ &(\Phi)_s = O \\ &\varepsilon_o \langle \vec{F}_s \cdot \vec{F}_r^* \rangle = \varepsilon_o \langle \Phi_s \Phi_r \rangle = \delta_{sr} \; . \end{aligned} \tag{4}$$

The fields $\vec{E}$ and $\vec{H}$, the current density $\vec{J}$ and the space charge density q are expanded as follows

$$
\begin{aligned}
\vec{E} &= A_i \vec{E}_i + C_s \vec{F}_s \\
\vec{H} &= B_s \vec{H}_s \\
\vec{J} &= D_i \vec{E}_i + G_s \vec{F}_s \\
q &= \varepsilon_o \mathcal{K}_s k_s^2 \xi_s ,
\end{aligned}
\tag{5}
$$

where repeated index in a product means summation over that index. Introducing these expansions into equation system (1) and using the orthogonal properties of the functions defined in (3) and (4), we find the following relations

$$
\begin{aligned}
&\omega_i A_i - \omega B_i = 0 \\
&\omega_i B_i - \omega A_i - \frac{D_i}{j\varepsilon_o} = j\omega S_i \\
&k_s \mathcal{K}_s = \frac{G_s}{j\omega\varepsilon_o} = - C_s
\end{aligned}
\tag{6}
$$

where the coefficient S_i prescribes the source of the i^{th} mode due to the coupling between the cavity and the waveguide. A result of these equations is

$$
A_i = \frac{jS_i}{\left(\dfrac{\omega_i}{\omega}\right)^2 - 1 - \dfrac{D_i}{j\omega\varepsilon_o A_i}}
\tag{7}
$$

which, with the definition of the coefficients, can also be written as

$$
A_i = \frac{jS_i}{\left(\dfrac{\omega_i}{\omega}\right)^2 - 1 - \dfrac{\langle \vec{J}\cdot\vec{E}_i^{\,*}\rangle}{j\omega\varepsilon_o \langle \vec{E}^{*}\cdot\vec{E}_i^{\,*}\rangle}} .
\tag{8}
$$

Introducing these results into Poynting's equations, we see that

$$
\langle \vec{E} \times \vec{H}^{*} \rangle_s = - j\omega \frac{S_i S_i^{*}}{\dfrac{\omega_i}{\omega}^{2} - 1 - \dfrac{\langle \vec{J}\cdot\vec{E}_i^{\,*}\rangle}{j\omega\varepsilon_o \langle \vec{E}\cdot\vec{E}_i^{\,*}\rangle}} .
\tag{9}
$$

To use the above formulas in measuring electromagnetic material properties, we need a relation between current density $\vec{J}$ and the cavity field $\vec{E}$. We first introduce a lossy plasma into the cavity and afterwards a small lossless dielectric sphere.

The plasma case

The standard formulas describing the plasma influence on the cavity resonances consider only one mode. Because the plasma is never uniform and does not fill the cavity, and because plasma waves are excited whenever the electric field has components parallel to the electron density gradient, we find that it is necessary to introduce additional modes, both irrotational and rotational. We illustrate this situation by introducing a lossy non-uniform plasma into the cavity.

An adequate relationship between the current density $\vec{J}$ and the electric field $\vec{E}$ for the plasma is obtained from the moment equations generated from the Boltzmann's transport equation. Since the ions can be assumed stationary, we write the resulting momentum balance equation for the electrons in the plasma as

$$(j\omega + \nu_m)\vec{J} + c_m^2 \vec{\nabla} q = \varepsilon_o \omega_p^2 \vec{E} \tag{10}$$

where ν_m is the electron collision frequency, c_m the velocity of acoustical waves in the electron gas, q the free space charge density associated with the plasma waves, and ω_p is the plasma frequency defined by

$$\omega_p^2 = \frac{e^2 n}{m\varepsilon_o} . \tag{11}$$

Introducing the series expansions (5) and (10) and using the relations (6) as well as of the orthogonal properties of the basis functions we find the following equation system for the coefficients A_i and C_s

$$A_i \left\{ \left(\frac{\omega_i^2}{\omega^2} - 1 \right) \delta_{ij} - \frac{\langle \omega_p^2 \rangle_{ij}}{j\omega(j\omega+\nu_m)} \right\} - C_s \frac{\langle \omega_p^2 \rangle_{sj}}{j\omega(j\omega+\nu_m)} = jS_j \tag{12}$$

and

$$C_s \left\{ \left[j\omega(j\omega+\nu_m) + c_m^2 k_s^2 \right] \delta_{sr} + \langle \omega_p^2 \rangle_{sr} \right\} = - A_i \langle \omega_p^2 \rangle_{ir} \tag{13}$$

where

$$\langle \omega_p^2 \rangle_{ij} \equiv \frac{\langle \omega_p^2 \vec{E}_i \cdot \vec{E}_j^* \rangle}{\langle \vec{E}_i \cdot E_i \rangle}$$

$$\langle \omega_p^2 \rangle_{ri}^* \equiv \langle \omega_p^2 \rangle_{ir} \equiv \frac{\langle \omega_p^2 \vec{E}_i \cdot \vec{F}_r^* \rangle}{\langle \vec{E}_i \cdot \vec{E}_i^* \rangle} \tag{14}$$

$$\langle \omega_p^2 \rangle_{sr} \equiv \frac{\langle \omega_p^2 \vec{F}_s \cdot \vec{F}_r^* \rangle}{\langle \vec{F}_s \vec{F}_s^* \rangle} .$$

Assuming that the coupling coefficients S_j and the plasma configuration are known, it is possible to determine all coefficients A_i and C_s from the equation system (12) and (13), and hence the actual field distribution in the cavity with the plasma. Because it is computationally impractical* we limit ourselves to some specific illustrative cases. First we assume that only the a^{th} solenoidal mode is excited and neglect the presence of all other solenoidal modes as well as all irrotational modes. Equation (12) then gives

$$A_a = \frac{j S_a}{\frac{\omega_a^2}{\omega^2} - 1 + \frac{1 + j\gamma}{1+\gamma^2} \frac{\langle \omega_p^2 \rangle_{aa}}{\omega^2} + \frac{j}{Q_a}} \tag{15}$$

with

$$\gamma \equiv \frac{\nu_m}{\omega} \tag{16}$$

* The above normal mode expansion which is in terms of the cavity modes is likely to be very slowly convergent. To get good convergence, it is probably necessary to get explicitly the actual waves in the plasma first and then determine the coupling to the cavity modes.

and where the term containing Q_a has been added in order to account for losses in the a^{th} solenoidal mode, due to the cavity itself and due to the influence of external circuit coupled to the cavity. This formula is currently used to interpret the plasma measurements with a microwave cavity. It is used two ways: by measuring the frequency shift and the attenuation at the actual resonance or by measuring the phase shift and attenuation at the resonance frequency of the empty cavity.

The resonance frequency is experimentally identified as the frequency ω_r where the amplitude of A_a is a maximum. Assuming that the coupling coefficient S_a and the Q_a are independent of the frequency one finds that ω_r to the first and second order is determined by the equation

$$\left(\frac{\omega_a}{\omega_r}\right)^2 - 1 = -\frac{1}{1+\gamma^2}\frac{\langle\omega_p^2\rangle_{aa}}{\omega_a^2}\left\{1+\frac{3\gamma}{2}\left(\frac{\gamma}{1+\gamma^2}\frac{\langle\omega_p^2\rangle_{aa}}{\omega_a^2}+\frac{1}{Q_a}\right)\left(1-\frac{2}{3}\frac{\gamma^2}{(1+\gamma)}\right)\right\} . \tag{17}$$

A linear relationship between the electron density and the frequency shift is therefore obtained only if

$$\frac{\Delta\omega}{\omega_r} = \frac{\omega_r-\omega_a}{\omega_a} = \frac{1}{2(1+\gamma^2)}\frac{\langle\omega_p^2\rangle_{aa}}{\omega_a^2} << 1 \tag{18}$$

and

$$\frac{3\gamma}{2}\left(1-\frac{2}{3}\frac{\gamma^2}{1+\gamma^2}\right)\frac{\langle\omega_p^2\rangle_{aa}}{\omega_a^2} << 1 . \tag{19}$$

Thus, the maximum electron density measured with the frequency shift method depends on how large error one can tolerate.

Since the chosen frequency in the phase shift and amplitude method is ω_a it follows that

$$\frac{1}{A_a} = \frac{1}{S_a}\left\{\frac{1}{Q_a}+\frac{\gamma}{1+\gamma^2}\frac{\langle\omega_p^2\rangle_{aa}}{\omega_a^2} - j\frac{1}{1+\gamma^2}\frac{\langle\omega_p^2\rangle_{aa}}{\omega_a^2}\right\} = \frac{1}{A}\,e^{-j\varphi} \tag{20}$$

where A is the amplitude of A_a and φ its phase angle. Therefore,

$$\gamma = \frac{\left(\cos\varphi - \frac{A}{A_o}\right)}{\sin\varphi} \tag{21}$$

and

$$\frac{\langle\omega_p^2\rangle_{aa}}{\omega_a^2} = \frac{(1+\gamma^2)}{Q_a}\,\frac{A}{A_o}\,\sin\varphi \tag{22}$$

where

$$A_o = S_a Q_a . \tag{23}$$

This method requires a measurement of Q_a and a procedure that assures that the measurement frequency is equal to ω_a. Errors associated with these measurement processes are discussed in Appendix C.

Formulas (15) and (23) apply only when one can neglect all other modes. We now illustrate the effects of the coupling between the solenoidal mode used for the measurements and all other solenoidal modes. We assume that the a^{th} mode is the lowest solenoidal mode, label it with 1 and consider its coupling to the j^{th} solenoidal mode. Equation (12) gives us the following equation for the determination of A_1.

$$A_1\left\{\frac{\omega_1^2}{\omega^2}-1+\frac{1}{1-j\gamma}\frac{\langle\omega_p^2\rangle_{11}}{\omega^2}\right\}+A_j\frac{\langle\omega_p^2\rangle_{j1}}{(1-j\gamma)\omega^2}=j\,S_1\,. \tag{24}$$

Assuming that the measurement frequency ω is very close to ω_1 we assume that

$$\omega^2\sim\omega_1^2<\omega_j^2>\langle\omega_p^2\rangle_{1j}>\langle\omega_p^2\rangle_{ij}$$

$$A_1>A_i,\qquad i,\quad j>1 \tag{25}$$

giving the following approximate equations for the determination of the coefficients A_j

$$A_j=jS_j\frac{\omega^2}{\omega_j^2}-A_1\frac{\langle\omega_p^2\rangle_{1j}}{(1-j\gamma)\,\omega_j^2}. \tag{26}$$

Introducing this result into (24) we find then that the coefficient A_1 can be written as

$$A_1=\frac{j\,S_1\left\{1-\frac{C_1}{1-j\gamma}\frac{\langle\omega_p^2\rangle_{11}}{\omega_1^2}\right\}}{\left\{\frac{\omega_1^2}{\omega^2}-1+\frac{1}{(1-j\gamma)}\frac{\langle\omega_p^2\rangle_{11}}{\omega^2}-\frac{C_2}{(1-j\gamma)^2}\left(\frac{\langle\omega_p^2\rangle_{11}}{\omega\,\omega_1}\right)^2+\frac{j}{Q_a}\right\}} \tag{27}$$

with the coefficients C_1 and C_2 defined by

$$C_1=\sum_{i>1}\frac{S_i}{S_1}\frac{\omega_1^2}{\omega_i^2}\frac{\langle\omega_p^2\rangle_{i1}}{\langle\omega_p^2\rangle_{11}} \tag{28}$$

$$C_2=\sum_{i>1}\left(\frac{\omega_1}{\omega_i}\right)^2\frac{\langle\omega_p^2\rangle_{1i}\langle\omega_p^2\rangle_{i1}}{\langle\omega_p^2\rangle_{11}^2}\;. \tag{29}$$

The Q_a for the empty cavity has again been inserted in order to make the amplitude of A_1 finite in the absence of the plasma. Note that both coefficients C_1 and C_2 are independent of the electron density; C_1 is a function of the plasma density configuration and the coupling mechanisms to the cavity and C_2 is only a function of the plasma configuration. Both these coefficients express the effects of the coupling between the 1st solenoidal mode, which is used in the measurements, and the higher solenoidal modes. Both coefficients are identically equal to zero if the plasma fills the cavity uniformly.

An inspection of formula (27) shows, for the frequency shift method, that the coupling to higher solenoidal modes can be neglected provided

$$1>>\frac{C_2}{(1-j\gamma)}\frac{\langle\omega_p^2\rangle_{11}}{\omega_1^2}\,. \tag{30}$$

This criterion depends on the mode and plasma configurations and is always violated when the plasma becomes dense. The criterion for the neglect of the coupling to the higher solenoidal modes is more stringent for the phase and amplitude method because not only (30) must be satisfied but it is also necessary that

$$1>>\frac{C_1}{(1-j\gamma)}\frac{\langle\omega_p^2\rangle_{11}}{\omega_1^2}\,. \tag{31}$$

The latter may unfortunately be more limiting than (30) because C_1 is both a function of the mode and plasma configurations and a function of the coupling mechanisms (loop, iris). This occurs when the coupling coefficients to one or more of the higher solenoidal modes are larger than the coupling coefficient to the fundamental mode used for the measurements.

Finally, we demonstrate the effects of the coupling to the irrotational modes. Again a general solution is impractical and we consider, as illustration, the case where the lowest solenoidal mode, labeled with index 1, couples to the r^{th} irrotational mode. The solution for the coefficient A_1 derived from the corresponding form of equations (12) and (13) can then be written as

$$A_1 = \frac{jS_1}{\left\{\frac{\omega_1^2}{\omega^2} - 1 + \frac{1}{1-j\gamma}\frac{\langle\omega_p^2\rangle_{11}}{\omega^2} + \delta_r + \frac{j}{Q_a}\right\}} \tag{32}$$

where

$$\delta_r = \frac{\langle\omega_p^2\rangle_{1r}\langle\omega_p^2\rangle_{r1}}{(1-j\gamma)\,\omega^2\left\{\omega^2(1-j\gamma) - \langle\omega_p^2\rangle_{rr} - c_m^2 k_r^2\right\}} \tag{33}$$

accounts for the influence on the fundamental solenoidal mode of the coupling to the r^{th} irrotational mode. The coupling coefficient is by definition written as

$$\langle\omega_p^2\rangle_{1r} \equiv \frac{\langle\omega_p^2\vec{E}_1\cdot\vec{F}_r^*\rangle}{\langle\vec{E}_1\cdot\vec{E}_1^*\rangle} \equiv -\frac{1}{k_r^*}\frac{\langle\phi_r^*\vec{E}_1\cdot\vec{\nabla}\omega_p^2\rangle}{\langle\vec{E}_1\cdot\vec{E}_1^*\rangle} \tag{34}$$

showing that the irrotational modes are excited only if the electric field, or a component of it, is parallel with the electron density gradient. The irrotational modes are, therefore, not excited if the plasma fills the cavity uniformly. In most practical situations, where the plasma is non-uniform, one must however expect irrotational modes to be excited. The influence of an irrotational mode is largest at its resonance, which occurs when

$$\omega^2 - \langle\omega_p^2\rangle_{rr} - c_m^2 k_r^2 = 0 \tag{35}$$

leading to

$$\delta_r = j\,\frac{\langle\omega_p^2\rangle_{1r}\langle\omega_p^2\rangle_{r1}}{\gamma\,\omega^2\langle\omega_p^2\rangle_{11}}\;. \tag{36}$$

Introducing this form of δ_r into expression (32) one finds that the criterion for when one may neglect the presence of irrotational modes, can be written as

$$1 >> \frac{\langle\omega_p^2\rangle_{1r}\langle\omega_p^2\rangle_{r1}}{\gamma\,\omega^2\langle\omega_p^2\rangle_{11}}\;. \tag{37}$$

It is important to notice, in view of the form of δ_r at resonance, that the irrotational mode will, for γ less than unity, show up as a change in the measured loss mechanism, while, for γ larger than unity, it will primarily influence the measured phase shift or frequency shift. It is in this connection important to point out that the density of resonances in the coupling to the irrotational modes is much larger than the density of resonances in the solenoidal modes because the former density is determined by the thermal velocity of the electrons while the latter is determined by the velocity of light. It is, therefore, very likely that the measurements are more strongly influenced by the presence of irrotational modes than by the presence of higher solenoidal modes.

In order to be able to view the microwave cavity method as a reliable method for measuring the plasma parameters, whether one uses the frequency shift or the phase and amplitude shifts, it is necessary to ascertain linearity between the desired parameter and the actually measured quantity. Three different mechanisms contribute to the deviation from the linearity, namely:

1) The intrinsic loss mechanism of the plasma itself as illustrated by formula (17). This mechanism affects essentially only the frequency shift method,

2) Coupling to the higher solenoidal modes as illustrated by formula (27). This mechanism not only contributes to deviations from linearity but may, under unfortunate circumstances, also change the proportionality factor in the linear range, and

3) Coupling to irrotational modes as shown by formula (32). Because of the high mode density of this mechanism, it is likely that it is most important for the determination of the upper limit of the linear range.

Unfortunately, the limits depend on the actual cavity design (not the idealized version), on the coupling mechanisms (iris, loop) used to connect cavity to wave guide, as well as on the shape of the plasma and the electron temperature. In general the models used for the evaluation of the limits are incomplete and do not allow adequate numerical evaluation. Therefore, it is most desirable to demonstrate the linearity and the limits of the linear ranges through calibration procedures.

The test sphere

We introduce a small sphere of pure lossless dielectric material with the dielectric constant ε into the cavity. We assume that the radius ρ of the sphere is sufficiently small compared to the dimensions of the cavity so that the sphere, wherever it is located, can be assumed to be in an essentially uniform electric field. Using a purely electrostatic theory [17] it is then easily shown that field inside the sphere can be written as

$$\vec{E} = \frac{3\varepsilon_o}{2\varepsilon_o + \varepsilon} \vec{E}_a \tag{38}$$

where E_a is the field at the location of the sphere but in the absence of the sphere. The frequency of this field is ω; and neglecting magnetic field effects one can then write the equivalent current density inside the sphere as

$$\vec{J} = j\,\omega\,(\varepsilon - \varepsilon_o)\,E = j\,\omega \frac{3\varepsilon_o(\varepsilon-\varepsilon_o)}{2\varepsilon_o + \varepsilon} \vec{E}_a \quad . \tag{39}$$

The resonance frequency of the a^{th} mode in the lossless case, according to (8), is determined by

$$\frac{\omega_a^2}{\omega^2} - 1 - \frac{\langle \vec{J}\cdot\vec{E}_a^{\,*}\rangle}{j\omega\varepsilon_o \langle \vec{E}_a\cdot\vec{E}_a^{\,*}\rangle} = 0 \quad . \tag{40}$$

Introducing the current density from (39) one finds that

$$\frac{\omega_a^2}{\omega^2} - 1 = \frac{3(\varepsilon - \varepsilon_o)}{2\,\varepsilon_o + \varepsilon} \quad \frac{E_a^2}{\langle E_a^2 \rangle} \quad \frac{4\pi\rho^3}{3} \, . \tag{41}$$

The frequency shift due to the insertion of the test sphere is proportional to the square of the electric field at its location. The test sphere can, therefore, be used for measuring the electric field distribution provided the electric field does not vary significantly within the volume replaced by the sphere. In the general case one has

$$\left(\frac{\omega_a}{\omega}\right)^2 - 1 = C \left(\frac{E}{E_o}\right)^2 \tag{42}$$

where E is the electric field at any point and E_o a normalized field. The constant C is in the particular case of the TM_{010} mode written as

$$C = 14.8 \; \frac{\rho^3}{hR^2} \; \frac{(\varepsilon - \varepsilon_o)}{(2\varepsilon_o + \varepsilon)} \tag{43}$$

where H is the height of the cylindrical cavity, R its radius and E_o the field at the center of the cavity.

Appendix B

Field distribution measurements in the cavity

To transform the cavity measurements into correct plasma parameters it is necessary to know the actual spatial distribution of the electric fields which interact with the plasma. This means that one should know the field distribution in the absence of the plasma and also how the field distribution is changed due to the plasma. Because the plasma is generally unknown, it is impossible to predict quantitatively the changes in the field distribution due to the plasma. Therefore, one must resort to perturbation theories [10] to interpret the measurements, that is, the measurements are understood only if the changes in the field can be neglected. To interpret the perturbation measurements it is still necessary to know the electric field distribution in the absence of the perturbation.

High Q cavities with simple geometries allow use of an analytic description of the electric field provided the couplings make negligible perturbations on the ideal cavity. If the ideal cavity is changed by the additions of holes, cut-off sleeves etc., to accommodate the plasma, then it is necessary to measure the electric field distribution for the mode used in the measurements. Such is the case for the ballistic range cavities.

The relative electric field at a point inside the cavity is measured by introducing a small test body at that point and by observing the resulting shift in the resonance frequency of the given mode. This frequency shift is proportional to the square of the electric field at the test point, provided the test body is a lossless dielectric material. Then the magnetic field influence is unimportant. The test body should be spherical to make the frequency shift independent of its orientation. A non-spherical test body can be used to measure the direction of the electric field. The sphere diameter times the gradient of the electric field should be small compared to the magnitude of the electric field. The formula (42) in Appendix A is then applicable. The coefficient C is determined by formula (43) provided the cavity is cylindrical and the mode TM_{010} is used for the measurements. To measure the relative field distribution it is not necessary to know the coefficient C.

The field measurements were done on the cavity shown in figure 3-1. The radius of the cylindrical part was 9" and the height 8". The cut-off sleeves had a radius of 2.75" and length of 8.375". The test sphere was made of alumina (Alsimag 748, L 715 C) and had a diameter of 0.5". The test sphere was attached to a monofilament nylon string with a diameter of 0.005". In the first set of measurements with this test body, the openings to the cut-off sleeves were covered with Al-foil to create the cylindrical cavity without the cut-off sleeves. A small hole was cut in the center of one of the Al-foils in order

to admit the test body into the cavity and to position it anywhere along the axis of the cavity. A similar hole was cut on the circumference of the cavity in order to allow the positioning of the test body along a diameter of the cavity. The frequency shift due to the insertion of the test body at various points along the axis or a diameter of the cavity were then measured. These results are seen in figure B-1. The measurements agree very well with the theoretical description of the electric field distribution

$$E_z = E_o J_o \left(r \frac{2.405}{R} \right)$$

for the TM_{010} mode of the ideal cavity. The axial measurements show a perfectly flat profile until the test body comes close to the walls where the perturbation theory breaks down. The radial field distribution agrees also very well with the field distribution for the ideal cavity as represented by the dashed curve. The difference between the dashed curve (theory) and the solid curve (measurements) is largest where the field gradients are largest, indicating that the test body is sensitive to the gradient of the field. The difference however is insignificant.

The same measurements were repeated after the Al-foils were removed and the cavity became sensitive to the presence of the cut-off sleeves. These measurements are shown in figure B-2. Obviously both the radial and the axial field distributions have changed due to the presence of the cut-off sleeves. The biggest change has taken place in the axial field distribution and the change is so large that the curvature, at the center of the cavity, of the axial field distribution is larger than that of the radial field distribution. This shows that one cannot neglect the axial coordinate dependence of the electric field, as has been done with the ballistic range cavities.

A third set of measurements shows how the quartz envelope of the plasma reference tube influences the electric field distribution of the cavity with cut-off sleeves. An open ended quartz tube with the same dimensions as that of the tube envelope was introduced coaxially into the cavity with the cut-off sleeves. Measurements were again done along the axis and along a center diameter. The measurements along the diameter were made possible by drilling holes, slightly larger than the test body, diametrically opposed to each other in the middle plane of the quartz tube. The results of these measurements are shown in figure B-3. The main change in the electric field distribution due to the presence of the quartz tube is found in the radial distribution. The field distribution within the quartz tube, in the symmetry plane perpendicular to the axis, is almost independent of the radius. The relative axial distribution of the field is essentially uninfluenced by the presence of the quartz tube.

The strong axial dependence and the change in the radial dependence of the electric field due to the insertion of the quartz tube are evidence for the presence of strong radial electric field components. The field distribution for the TM_{010} mode, generally used for unfolding the measured data into plasma parameters, has no radial electric field components. The true field distribution gives therefore a different filling factor (see Appendix A) than the assumed ideal field distribution. The filling factor depends not only on the electric field distribution, but also on the spatial distribution of the plasma. The treatment of the data obtained from the cavity with cut-off sleeves, neglects them and treats the cavity as if it contained a small diameter, axially uniform plasma. The difference between the real filling factor and the filling factor derived from the assumed field distribution is, in the case of the low density plasma, of the order of 10 per cent and generally insignificant relative to other errors. Errors due to the presence of substantial radial electric field components will be large when the plasma approaches the dense condition. The radial electric field components cause polarization effects at the boundary of the plasma which are likely to drastically change the fields within the plasma. These effects are difficult to evaluate numerically. The double perturbation method used in Appendix E shows how the polarization affects the measurements.

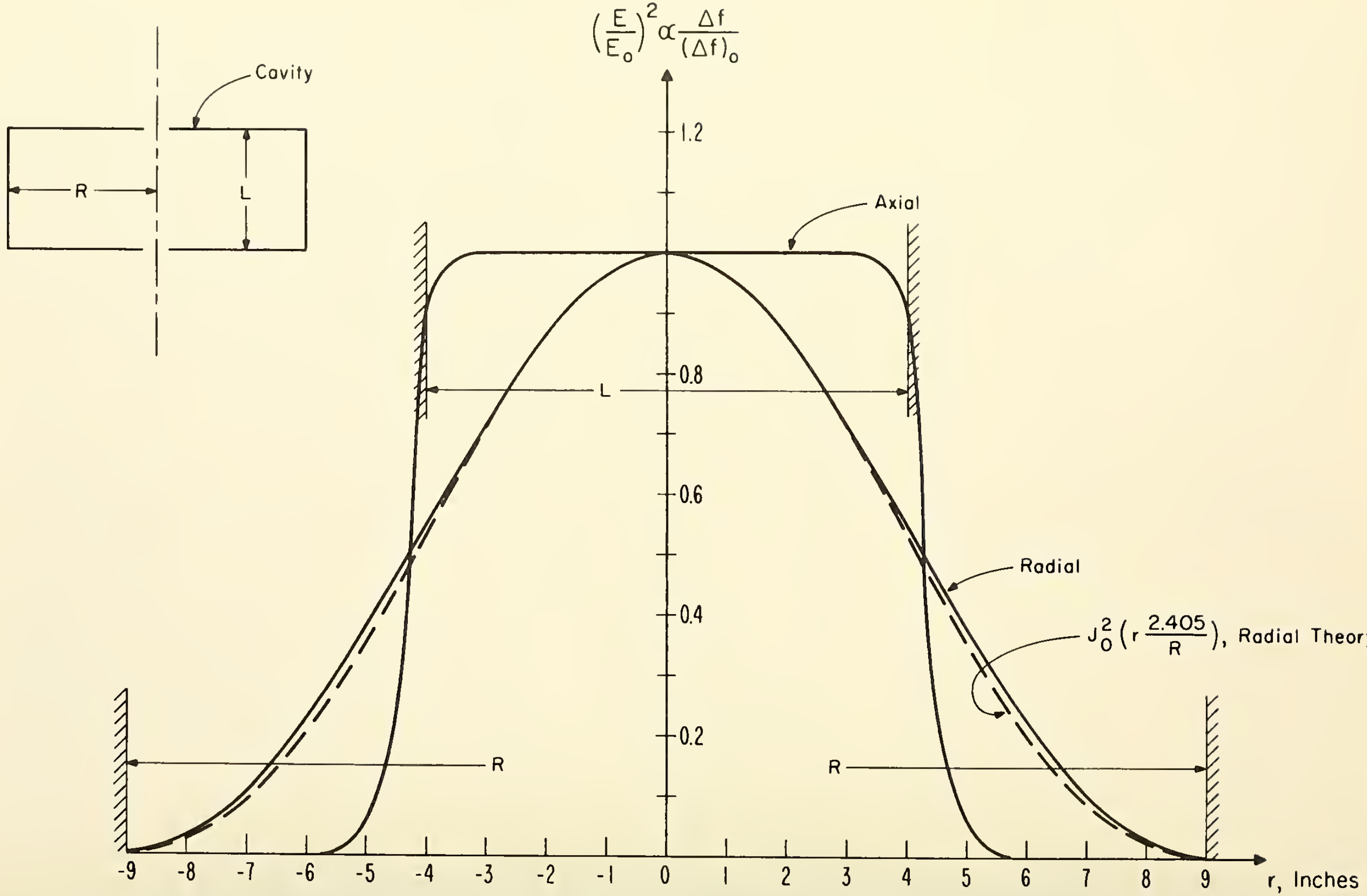

R = 9", L = 8", f_o = 500 MHz, $(\Delta f)_o$ = 66.5 kHz, 1/2" Aluminum Ball

Figure B-1. FIELD DISTRIBUTION, IDEAL CAVITY

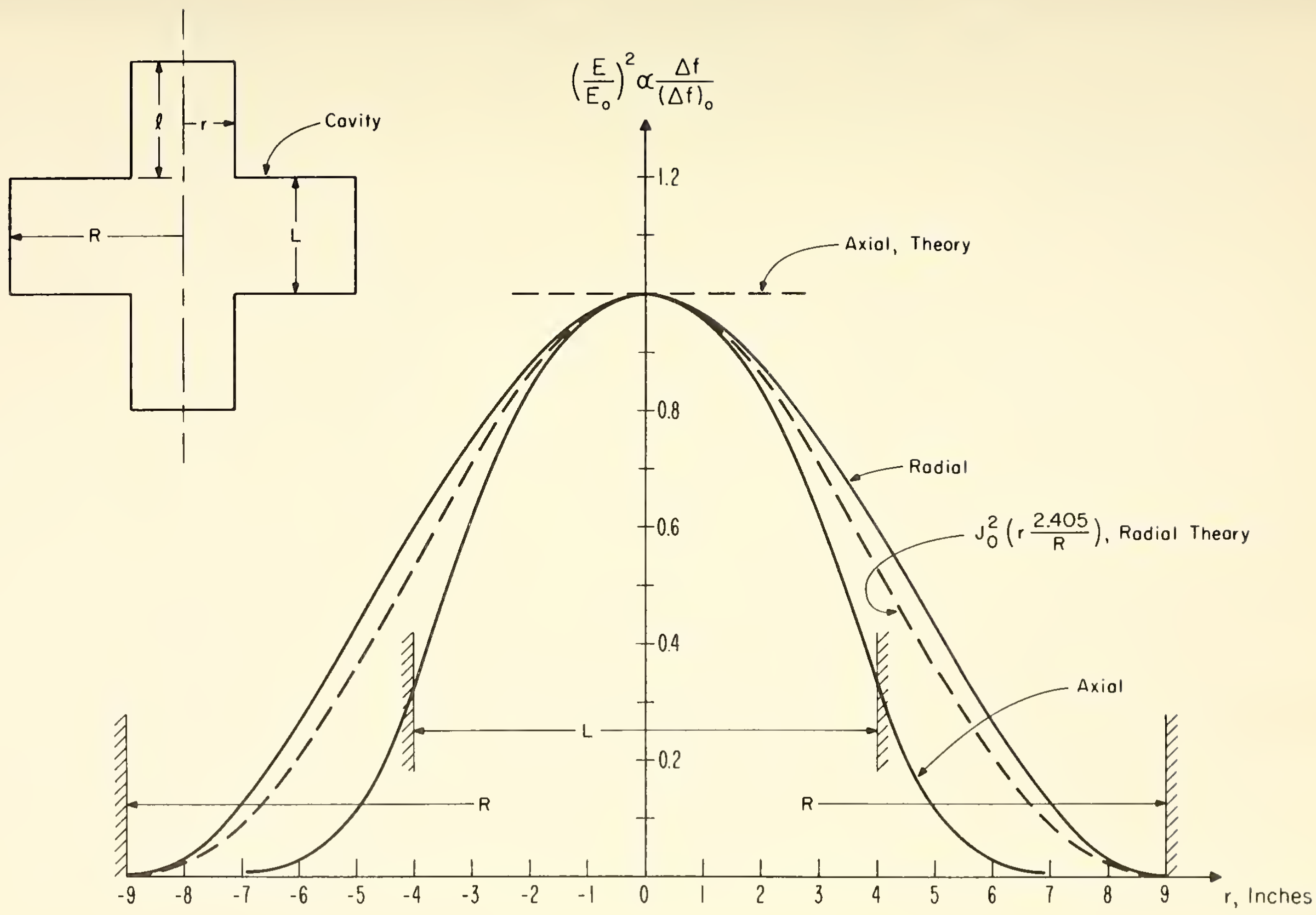

R = 9", L = 8", r = 2.75", ℓ = 8.375", f_o = 509 MHz, $(\Delta f)_o$ = 59 kHz

Figure B-2. FIELD DISTRIBUTION, CAVITY WITH CUT-OFF SLEEVES

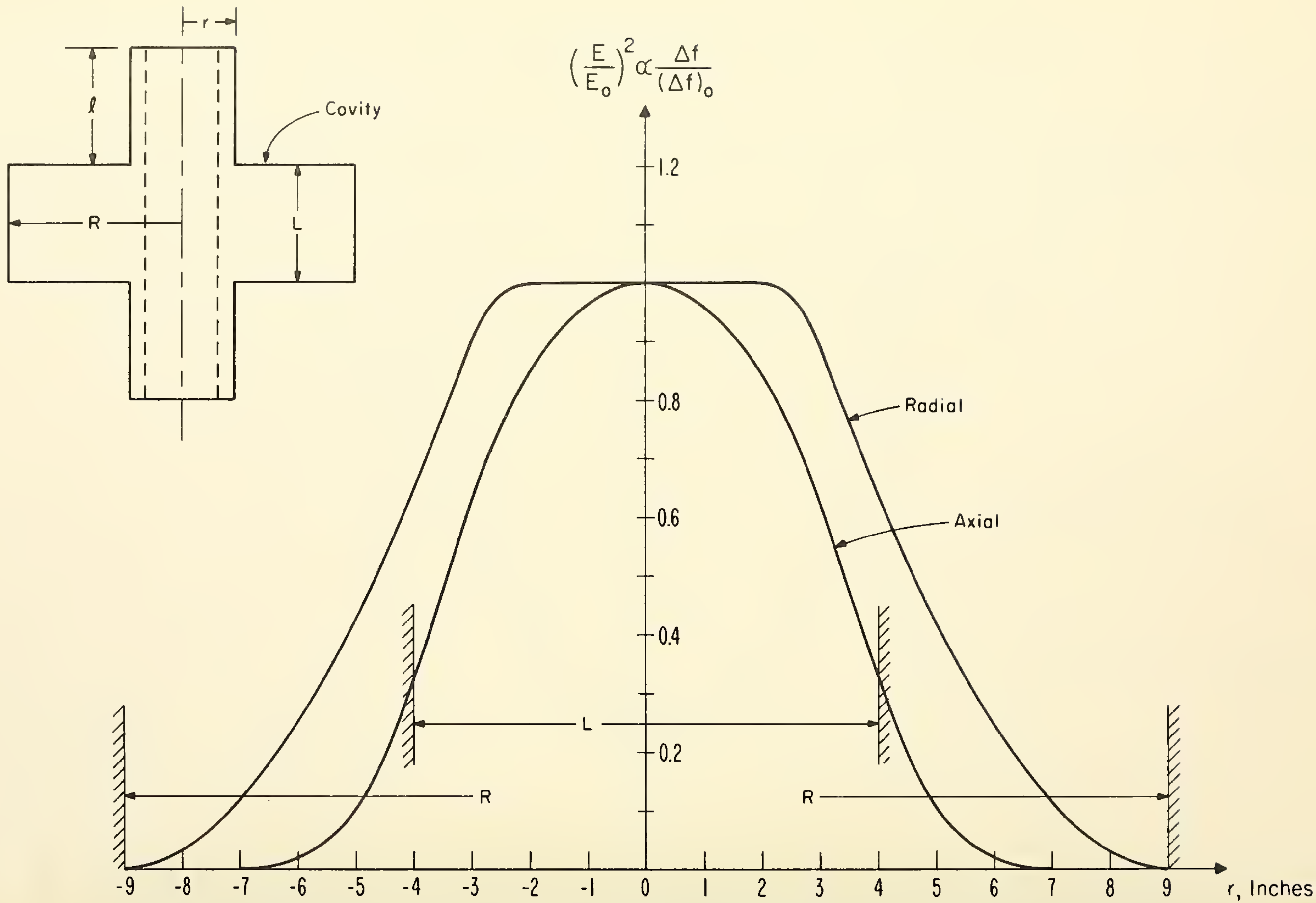

R = 9", L = 8", r = 2.75", ℓ = 8.375", f_o = 509 MHz, $(\Delta f)_o$ = 59 kHz

Figure B-3. FIELD DISTRIBUTION, CAVITY WITH QUARTZ TUBE

Appendix C

The influence of the microwave circuitry on the cavity measurements

The microwave cavity mode used for the measurements can be represented by a lumped circuit analogue if the interaction between the plasma and the microwave field is linear and if the overlapping of neighboring modes can be neglected. Figure C-1 shows the circuit. The signal generator is connected through an attenuator and a line segment to the cavity input. The output of the cavity is connected through a line segment to a matched impedance where the voltage measurements are done. The line segments have the characteristic impedance Z_o, the propagation constant k and the lengths ℓ_b and ℓ_d respectively. The attenuator has also the characteristic impedance Z_o. The current and voltage at the point a are related to the corresponding quantities at the point b in the following manner.

$$\begin{Bmatrix} i_a \\ \\ V_a \end{Bmatrix} = A_{ab} \begin{Bmatrix} i_b \\ \\ V_b \end{Bmatrix} \tag{1}$$

where the dyadic A_{ab} is defined as

$$A_{ab} = \begin{Bmatrix} \operatorname{Cos} \bar{\gamma}, & j \dfrac{\operatorname{Sin} \bar{\gamma}}{Z_o} \\ \\ j Z_o \operatorname{Sin} \bar{\gamma}, & \operatorname{Cos} \bar{\gamma} \end{Bmatrix} \tag{2}$$

where $\bar{\gamma} = -j\eta$ is purely imaginary and independent of the frequency. Similarly the dyadics for the two lossless line elements are

$$A_{bc} = \begin{Bmatrix} \operatorname{Cos} k\ell_b, & j \dfrac{\operatorname{Sin} k\ell_b}{Z_o} \\ \\ j Z_o \operatorname{Sin} k\ell_b, & \operatorname{Cos} k\ell_b \end{Bmatrix} \tag{3}$$

and

$$A_{de} = \begin{Bmatrix} \operatorname{Cos} k\ell_d, & j \dfrac{\operatorname{Sin} k\ell_d}{Z_o} \\ \\ j Z_o \operatorname{Sin} k\ell_d, & \operatorname{Cos} k\ell_d \end{Bmatrix} . \tag{4}$$

The simplest circuit analogue for the TM_{010} microwave cavity mode is shown in figure C-2 and is assumed to be symmetric with respect to the points c and d. The cavity mode is represented by the elements L, R and C. The couplings of the cavity to transmission lines are characterized by the impedance Z_1 and the mutual inductance M. The dyadic A_{cd} can therefore be written as

$$A_{cd} = \begin{Bmatrix} (1+DZ_1), & D \\ \\ Z_1(2+DZ_1), & (1+DZ_1) \end{Bmatrix} \tag{5}$$

2

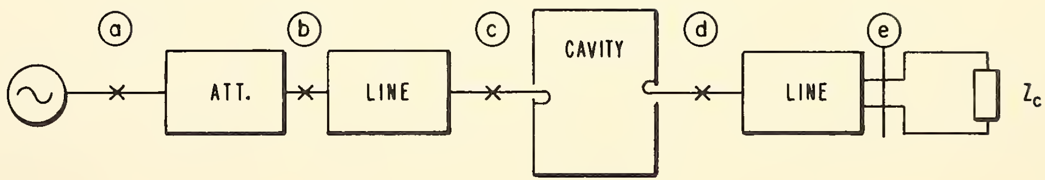

Figure C-1. THE CIRCUIT

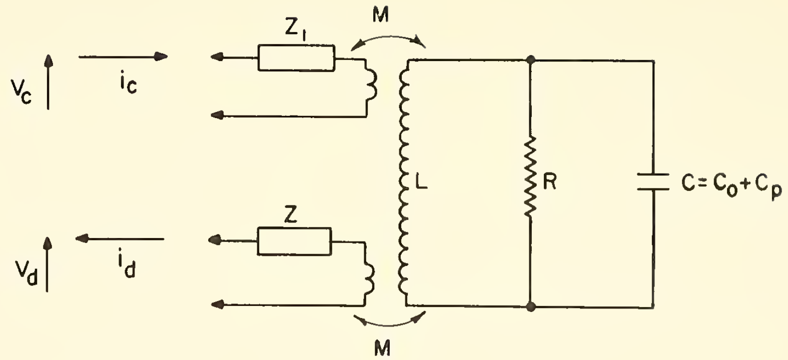

Figure C-2. THE CAVITY ANALOGUE

where

$$D = \frac{1}{\omega^2 M^2} \left(j\omega L + \frac{R}{1+j\omega RC} \right). \tag{6}$$

The capacitance C is the sum of two capacitances C_o and C_p, with C_p caused by the insertion of the plasma into the cavity. In order to simply relate the capacitance C_p to the plasma parameters we assume that we have a capacitance with the dimensions shown in figure C-3.The total area of a capacitor plate is A, while the distance between the plates is H. An effective cross section $\bar{a}$, smaller than A, is filled with a uniform plasma. The relative dielectric constant for the plasma can be written as

$$\epsilon_p = 1 - \left(1 + j\,\frac{\nu_m}{\omega}\right) \frac{\omega_p^2}{\omega^2 + \nu_m^2} \tag{7}$$

where

$$\omega_p = \sqrt{\frac{e^2 n}{m\epsilon_o}} \tag{8}$$

is the plasma frequency and where ν_m is the effective collision frequency for the electrons. It is easy to show that

$$\frac{C_p}{C_o} = - \frac{(1+j\gamma)}{1+\gamma^2}\, \beta \frac{\omega_p^2}{\omega^2} \equiv - (1+j\gamma)\,\delta \tag{9}$$

where

$$C_o \equiv \frac{\epsilon_o A}{H} \tag{10}$$

is the capacitance in the absence of the plasma, β the filling factor defined as

$$\beta = \frac{\bar{a}}{A}, \tag{11}$$

and

$$\gamma = \frac{\nu_m}{\omega}. \tag{12}$$

Assuming that δ, defined by (9), is much smaller than unity, that the unloaded Q of the cavity, defined as

$$Q_o = \omega_o RC_o \tag{13}$$

is much larger than unity, and that $\frac{\Delta\omega}{\omega} \lesssim 1\%$, we approximate the quantity D as

$$\frac{D}{D_o} = 1 + Q_o\gamma\delta + jQ_o\left(\frac{\omega^2}{\omega_o^2} - 1 - \delta\right), \tag{14}$$

where

$$\omega_o^2 = \frac{1}{LC_o} \tag{15}$$

$$D_o = \frac{1}{\omega_o^3 M^2 C_o Q_o}. \tag{16}$$

The currents and the voltages at the points a and e are related through the equation

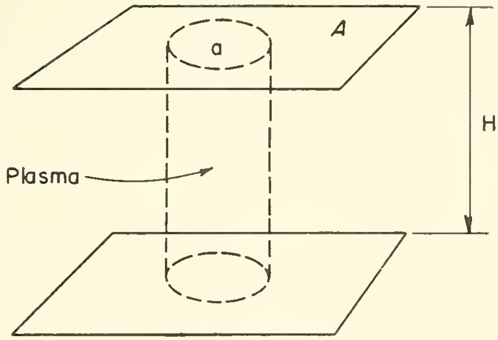

Figure C-3. THE CAVITY-PLASMA ANALOGUE

$$\begin{Bmatrix} i_a \\ V_a \end{Bmatrix} = A_{ab} A_{bc} A_{cd} A_{de} \begin{Bmatrix} i_e \\ V_e \end{Bmatrix} . \tag{17}$$

Terminating the chain with the characteristic impedance Z_o, that is, assuming that

$$V_e = i_e Z_o \tag{18}$$

it can be shown that the voltage ratio V_a/V_e can be written as

$$\frac{V_a}{V_e} = A + B \left(\frac{D}{D_o} - 1\right) \tag{19}$$

where

$$A = \left(1+r\right)\left(1+\frac{\alpha}{2}(1+r)\right)e^{\eta+js\left(\frac{\omega}{\omega_2}-1\right)} + \left(r-\frac{\alpha(1-r^2)}{2}\right)e^{-\eta-jm\frac{\omega}{\omega_3}-1} \tag{20}$$

and

$$B = \frac{\alpha(1+r)}{2}\left\{(1+r)\ e^{\eta+js\left(\frac{\omega}{\omega_2}-1\right)} - (1+r)\ e^{-\eta-jm\left(\frac{\omega}{\omega_3}-1\right)}\right\} \tag{21}$$

with

$$r = \frac{Z_1}{Z_o}, \quad \alpha = D_o Z_o, \ \gamma = -j\eta, \quad s = 2\pi \frac{\ell_b+\ell_d}{\lambda 2}, \ m = 2\pi \frac{(\ell_b-\ell_d)}{\lambda_3} . \tag{22}$$

The wave lengths λ_2 and λ_3, applicable for the transmission lines, and the corresponding frequencies ω_2 and ω_3, are chosen such that s and m are integers times 2π. The dimensionless parameters Q_o, r and α are design parameters for the cavity. The requirement that there are no reflections at the points c and d are expressed by the equation

$$\frac{D}{D_o} = \frac{2r}{\alpha(1-r^2)} . \tag{23}$$

Both α and D_o are by definition real. D and r are generally complex. Reflections at the points c and d are avoided at one frequency only, if at all.

The measurements are done at the frequency ω_1 which is in the close vicinity of the resonance frequency ω_o. Introducing V_{eo} for the voltage V_e in the absence of the plasma and V_{ep} for the same voltage in the presence of the plasma as well as assuming that the reference voltage V_a is uninfluenced by the insertion of the plasma and that Q_o is much larger than unity, one can show that

$$\left(\frac{V_{eo}}{V_{ep}} - 1\right) = \frac{Q}{1+jQ_L\epsilon_1} (\gamma-j)\,\delta \tag{24}$$

where

$$Q_L = \frac{B}{A} Q_o \tag{25}$$

and

$$\epsilon_1 = \left(\frac{\omega_1}{\omega_o}\right)^2 - 1 . \tag{26}$$

It is the purpose of the experiment to determine γ and δ. This is done by measuring the amplitude A and the phase angle θ of the voltage ratio $V_{ep}/V_{eo} = S\, e^{j\theta}$. It is assumed that Q_L is real and that ε_1 is sufficiently small so that its influence is negligible. One finds then that

$$\gamma = \frac{\nu_m}{\omega_1} = \frac{\cos\theta - S}{\sin\theta} \tag{27}$$

and

$$\delta = \frac{\beta}{1+\gamma^2} \frac{\omega_p^2}{\omega_1^2} = \frac{1}{Q_L} \frac{\sin\theta}{S} . \tag{28}$$

The electron collision frequency ν_m is determined by phase and amplitude measurements only. To obtain the electron density it is in addition necessary to determine the proportionality constant Q_L and the filling factor β. The Q_L, which in the ideal case is the loaded Q of the cavity and associated circuits, is determined from measurements of the resonance curves for the voltage ratio V_a/V_e in the absence of the plasma. This ratio can be written as

$$\frac{V_a}{V_e} = A\left\{1 + jQ_L\left(\frac{\omega^2}{\omega_o^2} - 1\right)\right\} . \tag{29}$$

When the measurements based on this formula are evaluated and long transmission lines are used, it is necessary to consider the fact that both A and Q_L are strongly frequency dependent. We consider this situation when the system is matched at the points c and d in the absence of the plasma and when $\omega = \omega_o$. This requirements leads to

$$\alpha = \frac{2r}{1-r^2} \tag{30}$$

giving

$$A = \frac{1+r}{1-r}\, e^{\eta + j s\left(\frac{\omega}{\omega_2} - 1\right)} \tag{31}$$

and

$$Q_L = rQ_o\left\{1 - \left(\frac{1-r}{1+r}\right) e^{-2\eta}\, e^{-j\left\{m\left(\frac{\omega}{\omega_3} - 1\right) + s\left(\frac{\omega}{\omega_2} - 1\right)\right\}}\right\} . \tag{32}$$

In the investigation of the consequences of deviations from the ideal situation where Q_L is real and frequency independent, it is convenient to rewrite Q_L in the form

$$Q_L = C\left\{1 - a\cos\left[b\varepsilon + c\right] + ja\sin\left[b\varepsilon + c\right]\right\} \tag{33}$$

$$\varepsilon_r = 2\left(\frac{\omega}{\omega_o} - 1\right) \simeq \left(\frac{\omega^2}{\omega_o^2} - 1\right) <<< 1 \tag{34}$$

$$C = rQ_o, \quad a = \left(\frac{1-r}{1+r}\right) e^{-2\eta}$$
$$b = \frac{\omega_o}{2}\left(\frac{s}{\omega_2} + \frac{m}{\omega_3}\right) \qquad c = m\left(\frac{\omega_o}{\omega_3} - 1\right) + s\left(\frac{\omega_o}{\omega_2} - 1\right) . \tag{35}$$

Assuming that c and $(b\varepsilon)$ are tuned to be less than a radian we can approximate Q_L as

$$Q_L = C\left\{1 - a + j\, a\, (c + \frac{b}{C}\; x\,)\right\} \tag{36}$$

and write the voltage ratio V_a/V_e as

$$\left(\frac{V_a}{V_e}\right) = A\left\{(a_o + a_1 x + a_2 x^2) + j(b_o + b_1 x)\right\} \equiv \frac{1}{\zeta} e^{-j\varphi} \tag{37}$$

with

$$\begin{aligned}
a_o &= 1 + \left[(1-a)\gamma + ac\right]\delta C & &\longrightarrow & &1 \\
a_1 &= -a(c - b\delta) & &\longrightarrow & &-ac \\
a_2 &= -\frac{ab}{C} & &\longrightarrow & &-\frac{ab}{C} \\
b_o &= -(1-a-ac\gamma)\delta C & &\longrightarrow & &0 \\
b_1 &= (1-a+ab\delta\gamma) & &\longrightarrow & &(1-a)
\end{aligned} \tag{38}$$

while

$$x = C\epsilon = C\left(\frac{\omega^2}{\omega_o^2} - 1\right). \tag{39}$$

We note that the ζ is the amplitude and φ is the phase shift of the signal. The arrows in (38) point to the forms for the coefficients in the absence of the plasma.

The measurements on the plasma are made at the resonance frequency of the system obtained in the absence of the plasma. This frequency is found by locating the maximum of the amplitude ζ, defined by (37), as function of the frequency. The resonance frequency of the ideal system would be located at the point $x = 0$. When neglecting terms x^3 and higher one finds from $\left|\frac{V_e}{V_a}\right|^2$ that the maximum actually is located at the point x_r given by

$$x_r = -\frac{a_o a_1 + b_o b_1}{a_1^2 + b_1^2 + 2a_o a_2} \xrightarrow[\delta \to o]{} \frac{ac}{(1-a)^2 + a^2c^2 - \frac{2ab}{C}}. \tag{40}$$

This formula shows that, in the simultaneous absence of attenuation (a approaching unity) and tuning of the lines (c different from zero), the presence of long transmission lines or other resonant structures (b very large), displace the resonance frequency of the system from the resonance frequency of the unloaded cavity. The magnitude of this shift can only be discovered by actually measuring the resonance frequency of the unloaded cavity and compare it with the resonance frequency of the system. One consequence of a significant difference between the two frequencies is that the proportionality coefficient Q_L becomes complex. Introducing x_r from (40) into (36) one finds that

$$Q_L = C\left\{(1-a) + jac\left(1 + \frac{ab}{C\left[(1-a)^2 + a^2c^2\right] - 2ab}\right)\right\}. \tag{41}$$

Only by tuning the lines such that the resonance frequency of the system becomes identical with the resonance frequency of the unloaded cavity ($c = 0$) or by introducing sufficient attenuation ($a << 1$) is it possible to make Q_L real.

In practice Q_L is obtained by measuring the frequencies ω'' and ω' of the half power points. Defining the apparent Q_L of the system as

$$Q_L' = \frac{2C}{x'' - x'} = \frac{2}{(\epsilon'' - \epsilon')} = \frac{2\omega_o^2}{\left[(\omega'')^2 - (\omega')^2\right]} \tag{42}$$

it is easily seen from (37) that

$$Q_L' = C \left\{ \frac{a_o^2+b_o^2}{a_1^2+b_1^2+2a_oa_2} - x_r^2 \right\}^{-\frac{1}{2}}$$

$$\xrightarrow[\delta \to o]{} C(1-a) \left\{ \sqrt{1-\frac{2ab}{C(1-a)^2}} + \frac{\frac{a^2c^2}{(1-a)^2}}{\sqrt{1-\frac{2ab}{C(1-a)^2}}} \right\} . \tag{43}$$

In the non-ideal system there may, therefore, be a considerable difference between the desired proportionality constant Q_L and the apparent proportionality constant Q_L'. In the case where the transmission lines are tuned to the resonance frequency of the unloaded cavity, the formula above simplifies to

$$\frac{Q_L'}{C(1-a)} \xrightarrow[\delta \to o]{} \sqrt{1-\frac{2ab}{C(1-a)^2}} . \tag{44}$$

Even in this case it is possible to have a discrepancy between Q_L and Q_L'. The correction term that appears under the square root sign of (44) is due to storage of energy outside the cavity but between the measuring points. This should properly be viewed as a correction to the filling factor β which has been calculated on the assumption that all stored energy is located inside the cavity.

If δ and γ are the true values to be measured, and δ' and γ' are the measured values obtained viewing the system as ideal, that is, if

$$\gamma' = \frac{\cos\theta - S}{\sin\theta} \tag{45}$$

and

$$\delta' = \frac{1}{Q_L'} \frac{\sin\theta}{S} \tag{46}$$

it is easily shown with equations (24) and (30) that the correct values of δ and γ are determined by the formulas

$$\delta = F_1 (1-F_2\gamma')\delta' \tag{47}$$

and

$$\gamma = \frac{(\gamma'+F_2)}{(1-\gamma'F_2)} \tag{48}$$

where

$$F_1 = \frac{Q_L'}{C(1-a)\left\{1+\frac{a^2}{(1-a)^2}(c+b\epsilon_r)^2\right\}} \xrightarrow[a,b,c \to]{} 1 , \tag{49}$$

and

$$F_2 = C\frac{a^2b}{(1-a)}(2c+b\epsilon_r)\epsilon_r^2 \xrightarrow[a,b,c \to o]{} 0 \tag{50}$$

The only actually measured quantities that appear in the formulas above are the phase angle θ, the amplitude ratio S, and Q_L', the apparent Q of the system. The quantities Q_L and x_r are generally unknown functions of the system parameters a, b, c and C. These functions are, in the particular case illustrated here, known functions only because the system is sufficiently simple to be amenable to analysis. The presently accepted measurement procedure gives neither information about these functions nor about the system parameters. Most systems, in particular complex systems, can therefore be expected to have systematic errors which may be very large. In the case illustrated here, large systematic errors appear if the parameter a approaches unity, which occurs when attenuation is lacking and the coupling to the cavity is strong.

To assure the correct determination of δ and γ, it is necessary to execute one of the following procedures:

1) Ascertain that the system is ideal by demonstrating, through measurements, that Q_L' is not significantly different from Q_L and that finiteness of ε_r does not introduce a significant error.

2) For the non-ideal system, determine the system parameters a, b, c, and C or their equivalents so that the complex proportionality constant Q_L and the displacement ε_r can be computed.

3) Calibrate the system through measurements on a known plasma or a suitable substitute.

Because the first two procedures are very complex, they should be avoided if the system can be calibrated.

The electron density, or properly speaking of the quantity δ, can also be determined by measuring the shift of the resonance frequency of the system due to the insertion of the plasma into the cavity. This method is simpler than the method based on the phase and amplitude measurements. Let $\omega_{r\delta}$ be the resonance frequency in the presence of the plasma and ω_{ro} the corresponding frequency in the absence of the plasma. It is then easily shown from (40) that

$$\left(\frac{\omega_{r\delta}}{\omega_o}\right)^2 - \left(\frac{\omega_{ro}}{\omega_o}\right)^2 = \varepsilon_{r\delta} - \varepsilon_{ro} = \frac{x_{r\delta} - x_{ro}}{C} = G_1 (1+G_2)\,\delta \tag{51}$$

where

$$G_1 = \frac{\left\{1 - \dfrac{ab}{C\left[(1-a)^2 + a^2c^2\right]}\right\}}{\left\{1 - \dfrac{2ab}{C\left[(1-a)^2 + a^2c^2\right]}\right\}} \xrightarrow[a,\,b,\,c\,\to\,o]{} 1 \tag{52}$$

and

$$G_2 = \frac{1}{C}\,\frac{4a^3bc^2}{\left[(1-a)^2 + a^2c^2 - \dfrac{ab}{C}\right]\left[(1-a)^2 + a^2c^2 - \dfrac{2ab}{C}\right]} \xrightarrow[a,\,b,\,c\,\to\,o]{} o\,. \tag{53}$$

In the ideal case when a and b are sufficiently small one finds therefore that

$$\delta = \left(\frac{\omega_{r\delta}}{\omega_o}\right)^2 - \left(\frac{\omega_{ro}}{\omega_o}\right)^2 \simeq \frac{2\Delta\omega}{\omega_o}\,. \tag{54}$$

It is important to point out that for high Q system where the parameter C is very large one can write

$$G_1(1+G_2) \simeq 1 + \frac{ab\left[(1-a)^2 + 5a^2c^2\right]}{C\left[(1-a)^2 + a^2c^2\right]} \tag{55}$$

showing that the frequency shift method permits larger deviations from the ideal system by allowing large values of the parameters a, b, and c. Because the frequency shift method need not measure a calibration constant for the determination of δ, it is more attractive than the previous method, which is based on a measurement of the phase, and amplitude as well as a proportionality constant.

The frequency shift method may also be used for measuring the electron momentum transfer collision frequency ν_m. It is then, of course, necessary to include a measurement of an attenuation as well as a measurement of the loaded Q of the system in the absence of the plasma. At resonance in the presence of the plasma and in the ideal case, it is easily shown with formulas (14) and (19) that

$$Y\delta = \frac{1}{Q_L} \quad \frac{1}{S'} - 1 \tag{56}$$

with

$$S' = \frac{V_{ep}}{V_{eo}} \tag{57}$$

where V_{ep} now is measured at the resonance of the system in the presence of the plasma and where V_{eo} is the corresponding quantity at resonance and in the absence of the plasma. Because one must measure both an attenuation and the loaded Q of the cavity, this measurement is subject to the same kind of errors as those in the phase and amplitude method.

Both the frequency shift method, and the method based on phase and amplitude measurements should give the same value for δ when the measurements are done on the same plasma. This fact can be used to calibrate the more complex systems. It is technically very simple to put together an ideal system for measuring δ with the frequency shift method. By using both methods simultaneously on the same reference plasma, one can find out whether the more complex system has systematic errors or not. It is not necessary to know the reference plasma parameters. They need only to be in the same range as those of the plasmas of interest.

Appendix D

The standard reference plasma

I. Description of the reference tube

A phenomenological description of the cold cathode low pressure DC discharge is given by von Engel[11]. Starting from the cathode of the DC discharge one observes the Aston dark space, the cathode glow, the cathode dark space, the negative glow, the Faraday dark space and finally the positive column, the anode dark space and anode glow. The electrons are generated on the cathode surface by ion and photon bombardment. They are accelerated through the Aston dark space, the cathode glow and the cathode dark space and constitute a fairly well defined beam when they arrive at the negative glow. Most of the negative glow characteristics are determined by the electron beam. The energy of the electrons is approximately equal to the cathode fall, the voltage difference between the cathode and the negative glow. The length of the negative glow is determined by the reaching distance of the electrons, and the Faraday dark space starts where the electron beam has lost its energy. The negative glow is essentially field free. Its electrons are generated by the beam. The absence of the field allows these electrons to cool rapidly and to be lost by electron-ion recombination.

The negative glow properties outlined above are approximate for the normal negative glow discharges when the cathode fall is only a few hundred volts. These properties are dominant when the discharge tube is operated in the abnormal glow region, where the cathode fall can be an order of magnitude larger than the normal cathode fall. A detailed description of the beam generated negative glow is given by Persson[12]. The best negative glow is found in pure helium which has the smallest ionization cross section and the minimum electron-ion recombination coefficient (the collisional radiative recombination process). The length of the negative glow region and its electron density are therefore larger in helium than in any other gas under comparable circumstances.

This abnormal negative glow in helium at 1 Torr pressure is ideally suited as a reference plasma for many reasons:

1. It is easier to introduce and maintain clean helium in a cleaned vacuum envelope than any other gas (by diffusion through a hot quartz tube). Hence the discharges in pure helium are more reproducible than other gases and/or mixtures.

2. A discharge tube with well chosen cathode material and tube design does not arc during the operation in the abnormal glow region. The operational life time and shelf life are then sufficient for the tube to be used as a reference plasma.

3. The abnormal negative glow in helium at 1 Torr pressure can be made several feet long with diameters in excess of 6 inches. The design and the operation of the tube are simple.

4. The intrinsic properties of the plasma are insensitive to the plasma dimensions when the length is less than the beam reaching distance and the radius is greater than the size of the diffusion dominated region.

5. The plasma can be generated in DC, AC and pulsed conditions without losing its basic properties.

6. A properly designed discharge tube operates as well, if not better, in a uniform magnetic field aligned with the tube axis.

7. Electron densities in excess of 10^{12} cm^{-3} can be reached with low power, about 100 Watts. The electron densities higher than 10^{13} cm^{-3} can be achieved but only at the expense of considerable power consumption and shortened tube life time.

8. The bulk of the electrons have a very low electron temperature, approximately 0.1 eV, and there is no significant ionization by thermal electrons. Thus, instabilities and oscillations typical of the positive column or arc type plasmas, which are maintained by ionization due to "thermal" electrons, are not present.

9. Since the ratio between the electron beam density and the plasma electron density is small, of the order 10^{-6}, and the corresponding velocity ratio is large, of the order 200, oscillations due to the two stream instability are not excited.

10. Due to lack of thermal excitation and ionization and because the majority of the excited electronic states are populated through the electron-ion recombination process, a Saha equilibrium is established for the higher excited states which allows accurate determination of the electron density and electron temperature by spectroscopic means.

11. The intrinsic steady state plasma properties differs very little from the "afterglow" plasma. This plasma is ideally suited for pulsed operations.

12. The pulsed operation of the plasma gives reproducible afterglow with the electron density varying, from 10^{12} cm^{-3} to 10^5 cm^{-3} or less.

Consequently, the abnormal negative glow in helium is a good standard reference plasma for the ballistic ranges. The tube design is shown in figure D-1. The tube dimensions were chosen to fit inside the "standard" cavity of the ballistic ranges, which has a resonance frequency of 450 Mc for the TM_{010} mode. The envelope is quartz with an inside diameter of 5 inches. The electrodes are high density, high purity graphite (POCO AXM-5Q1). The tube is symmetric so either electrode can be used as cathode, thereby doubling its life time. The distance between the electrodes is 20 inches.

Because proper operation makes it necessary to be careful in tube construction, a detailed discussion of the manufacturing procedure follows:

1. The original tubes were built with tungsten brush cathodes. These cathodes were used to discourage arc formation and arc spots on the cathodes when the tube is operated at the high voltages necessary for the abnormal negative glow plasmas. Because of the expense and complexities associated with the brush cathode, other designs and cathode materials were studied. The high density, high purity graphite is an excellent material for cold cathodes because it has a very low vapor pressure, essentially no melting, and very high boiling point which efficiently discourages the formation of arc spots. Because the sputtering rate is low, the graphite cathode can be a plane electrode without important loss in tube life time. To further discourage arc formation on plane electrodes, the cathode is closely fitted to the inside of the tube envelope without touching the glass. Tubes built with graphite electrodes have the advantage over tubes with metal electrodes because the carbon deposits sputtered onto the glass walls can be removed without destroying the tube: (1) By baking the tube or by heating the sputtered glass surfaces with a torch in the presence of added air or oxygen, (2) By adding a few percent oxygen to the helium, and running a discharge for a few hours. The resulting gas mixture is then pumped out and replaced by pure helium.

2. To obtain a reproducible and well defined abnormal negative glow in helium, it is important that the tube be processed using good, high vacuum technology. All parts of the tube should be cleaned and degreased. The cathode, in particular the graphite cathodes, must be pre-processed in a high vacuum furnace. The final vacuum stage to the tube must have traps preventing the oil from the diffusion pump and the forepump from reaching the tube. A vacuum of 10^{-10} Torr can and must be reached by the normal three stage glass constructed oil diffusion pumps. The helium is purified and fed into the discharge tube by a quartz diffusion leak located on the high vacuum side of the vacuum system. To remove surface impurities the discharge tube is filled to the desired pressure, the discharge is run for a short time, and the tube pumped and refilled with pure helium. The tube is then sealed and removed from the vacuum system.

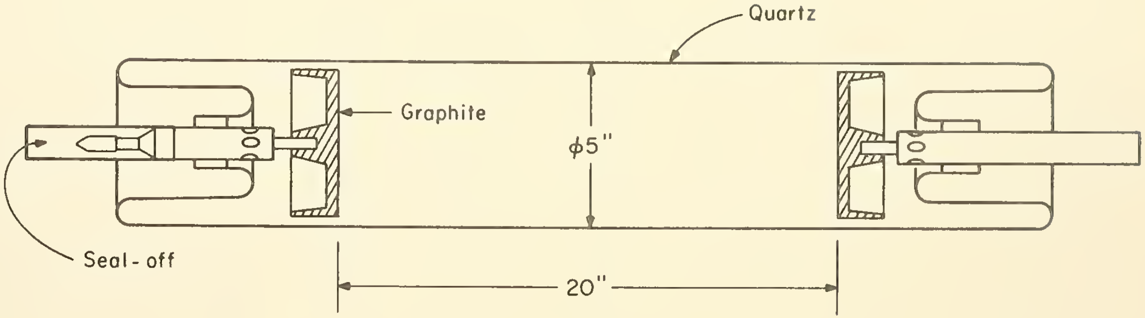

Figure D-1. THE STANDARD REFERENCE TUBE

3. If the tube has been processed correctly it is ready for immediate use after detachment from the vacuum system. Because the gas pressure will decrease with the use of the tube (clean-up due to sputtering) one must be able to measure the gas pressure of sealed off tubes. For a given tube size and well defined electrode material, the voltage-current characteristic is uniquely defined by the pressure. A set of voltage-current characteristics for the standard reference plasma tube are shown in figure D-2. It is obvious from these measurements that the characteristics are sensitive to pressure changes. In the reference plasma tube, the voltage-current characteristic measured after several months use show no measurable change from the characteristic measured when the tube was new.

If a gas discharge tube is to serve as a standard reference tube, it must satisfy several requirements. First, and most important, the manufacturing procedure and the processing methods must always give the same end product in terms of the desired measurements when the tube is new and it must have a long shelf life. All measurements on the abnormal negative glow in helium in the tube discussed have been reproducible within a few per cent and its shelf life is more than adequate, provided the prescription for its manufacture and processing as outlined above are followed. Second, it is necessary that the operational life time of the tube is sufficiently long so that many sets of reproducible measurements can be executed. The life time of the above tube, operated at 1 Torr pressure in helium and with a DC current of 50 mA, is estimated to be about 100 hours. This life time can be extended by one to two orders of magnitude by operating it in pulsed condition.

II. The use of the reference tube.

The reference standard tube for electron density measurements uses a current pulse of 50 mA of 10 msec duration, repeated every 200 msec. A typical set of measurements are shown in figure D-3. The electron density during the pulse and in the early afterglow was measured with a microwave interferometer at 35 GHz. The minimum measurable phase shift of the interferometer was approximately 0.2 degree corresponding to a minimum measurable electron density of approximately 10^{10} cm^{-3}. Electron densities below the range of the interferometer were measured with a cavity of the same type as the "standard cavity" of the ballistic ranges but with a slightly higher resonance frequency, 500 MHz, for the TM_{010} mode. The frequency shift method was used because it is least subject to systematic errors.

The electron densities plotted in figure D-3 were evaluated by assuming an ideal electric field distribution for the TM_{010} mode and that the electron density was axially uniform with the radial dependence described by the zeroth order Bessel function. These assumptions do not truely represent the physical situation. Early in the afterglow the electron-ion recombination process dominates, giving a spatial electron density distribution that is flatter than the zeroth order Bessel function. In the late part of the early afterglow the diffusion process dominates and the radial distribution of the electron density is correctly described by the zeroth order Bessel function. Thus, the conversion of the interferometer measurements into electron densities have a systematic error which approaches 50 per cent in the very early afterglow and is very likely to be negligible at the lower end of the interferometer measurements.

The conversion of the cavity measurements to electron densities generates complex systematic errors. Only for very low electron densities, where the plasma frequency is significantly lower than the resonance frequency of the TM_{010} mode is the simple perturbation theory applicable. The assumption that the electric field distribution is the ideal TM_{010} generates a systematic error because the real electric field distribution is quite different. This systematic error depends on the electron density and becomes progressively worse with increasing electron density.

The relative position of the two curves, the first based on the microwave interferometer data and the second on the cavity data, is uncertain due to the systematic errors. The relative systematic error is likely to be 10 to 30 per cent and to be largest in the range where the two curves overlap. This error can not be resolved except through a measurement method

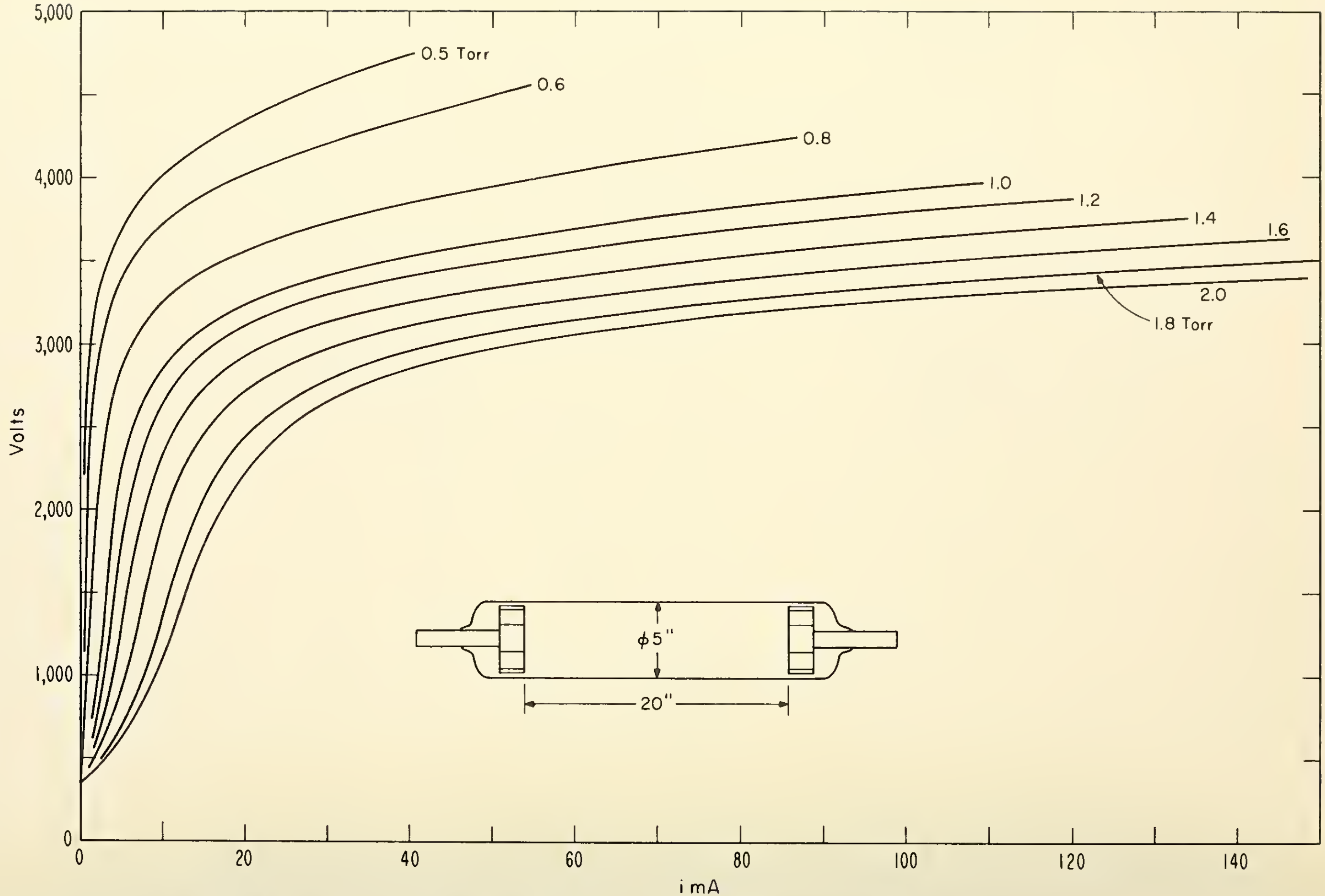

Figure D-2. V-i CHARACTERISTICS OF STANDARD REFERENCE PLASMA TUBE

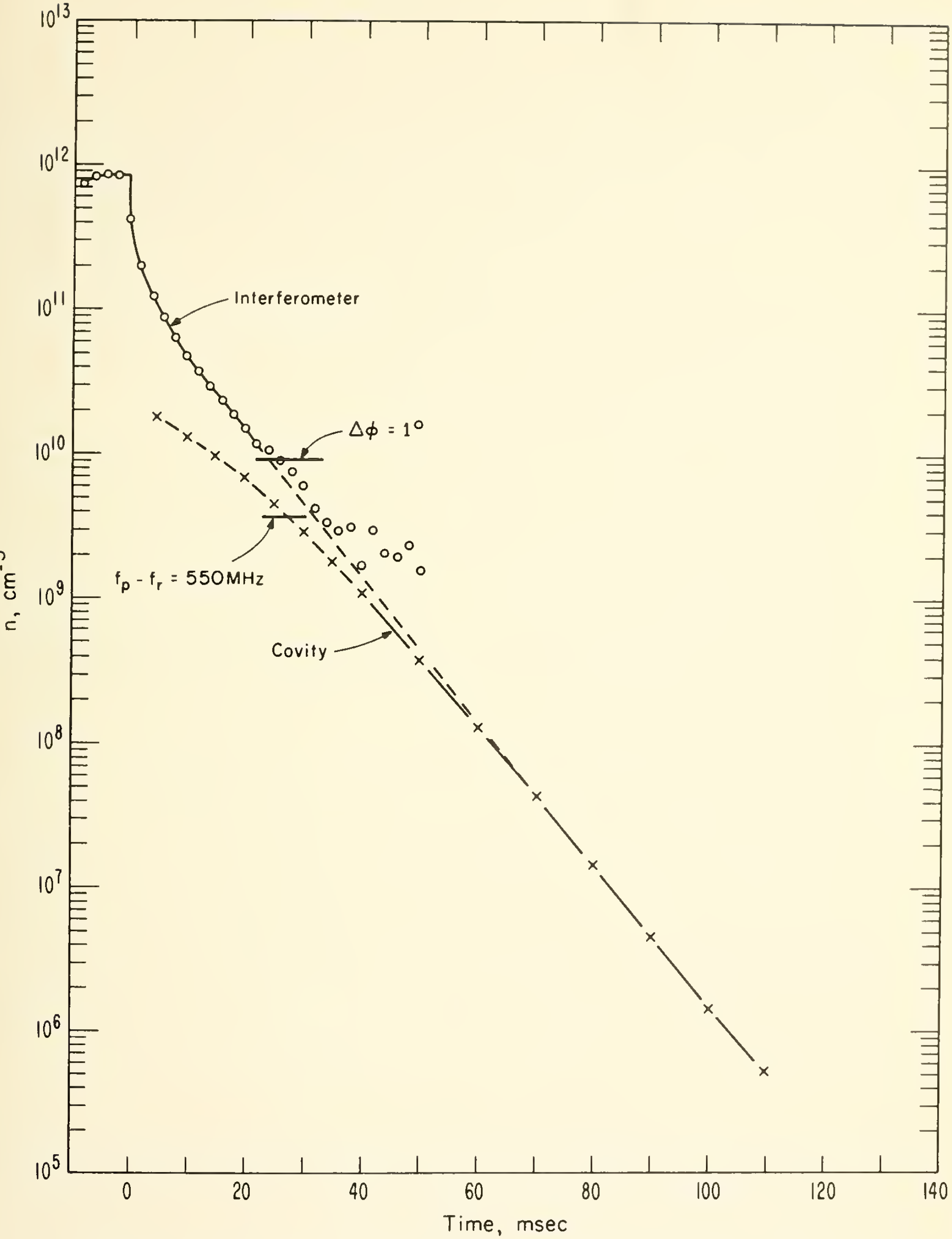

Figure D-3. Electron Density of Standard Reference Plasma Tube

that overlaps the methods used here. Nevertheless, the exceptional reproducibility of the measurements show that the abnormal negative glow is well suited for comparing different electron density measurement methods.

Appendix E

The effects of polarization in the plasma on measurements.

The most difficult problem associated with the microwave cavity measurements is the evaluation of the systematic errors due to polarization effects [13]. These become important when the plasma frequency approaches and exceeds the actual resonance frequency of the cavity. The electric polarization effects dominate, and occur when the electric field has substantial components parallel to the electron density gradients. Quantitative evaluation of these effects are difficult because neither the electric field nor electron density distributions are sufficiently well known to unfold the measurements or for an error estimate. Such is the case for "standard cavity" used in the ballistic ranges where the cut-off sleeves cause strong radial electric field components (see Appendix B) which are neglected in the usual evaluation of the data. It is simpler to demonstrate the presence of these errors experimentally.

The standard procedure for measuring the electric field distribution uses a small perturbing sphere. The microwave cavity used in the ballistic ranges, and the abnormal negative glow plasma used for its calibration, are both large enough to allow a small perturbing sphere within the plasma. It is then possible to measure the changes in the electric field inside the plasma due to the plasma. The insertion of a small sphere into the center of the plasma and the cavity shifts the resonance frequency for two reasons. First, a volume of the plasma equal to the volume of the sphere is displaced by a dielectric material with properties different from the plasma properties. This shift is proportional to the third power of the radius of the sphere and the square of the local electric field. A less obvious but more important shift happens because the surface of the sphere allows electrons and ions to recombine so fast that it acts like an infinite sink. The spatial distribution of the electrons and ions in the neighborhood of the sphere is therefore determined by the ambipolar diffusion to the surface of the sphere.

To model the effect of the test sphere on the electron density distribution we chose, for the sake of simplicity, a spherical cavity of radius R which is very large compared to the test sphere radius ζ. We assume that the spatial distribution of the plasma is determined by the ambipolar diffusion equation

$$\nabla^2 n + \frac{\nu_i}{D_a} n = 0 \tag{1}$$

where n, ν_i, D_a are the electron density, the ionization frequency, and ambipolar diffusion coefficients respectively. The spatial distribution of the electron density n without the test sphere is

$$n = n_o \frac{\operatorname{Sin} k_o r}{k_o r} \tag{2}$$

with

$$k_o R = \pi, \tag{3}$$

and with n_o the electron density at the center of the cavity. The introduction of the test sphere at the center of the plasma changes the coefficients and the spatial distribution to

$$n_p = C n_o \frac{\operatorname{Sin} k_p (r-\zeta)}{k_p r} \tag{4}$$

with

$$k_p (R-\zeta) = \pi \tag{5}$$

The electron density n_o and the coefficient C are undetermined. They can only be determined in the non-linear formulation,[14] where one also specifies the recombination rates of electrons and ions at the boundary surfaces. To bypass these difficulties, the electron density gradient at the boundary surface located at the radius R, is considered uninfluenced by the presence of the test sphere. One finds, by setting the electron density gradients at the radius R equal for the two cases, that the coefficient C is equal to unity. The change ΔN in the total number N of the electrons in the plasma, due to the insertion of the test body, is

$$\Delta N = 4\pi \int_{\zeta}^{R} r^2 (n_p - n)\, dr - \frac{4\pi \zeta^3}{3} n_o \tag{6}$$

which, if the distributions (2) and (4) are used and the coefficient C is equal to unity to the lowest order in (ζ/R) becomes

$$\Delta N = - \frac{4 n_o R^3}{\pi} \frac{\zeta}{R} \tag{7}$$

or

$$\Delta N = - C n_o \left(\frac{\zeta}{R}\right), \tag{8}$$

where C now is a different coefficient which depends on the configuration of the plasma. If the radius of the test sphere is made small enough, it follows that the frequency shift of the microwave cavity, due to the insertion of the test sphere into the center of the plasma, depends only on the change in the total number of electrons and is independent of the material in the test sphere. The frequency shift $\Delta\omega$ due to the insertion of the test sphere can then be written as

$$\frac{\Delta\omega}{\omega} = - C_1 n_o E_p^2 \frac{\zeta}{R} \tag{9}$$

where E_p is the local electric field, and n_o the local electron density, and where R represents an effective radius of the plasma, while C_1 is a coefficient which depends on the plasma and cavity configurations.

Figure E-1 shows the experimental arrangement used to investigate the plasma polarization effects induced by the cut-off sleeves. A long quartz tube with an inside diameter slightly larger than 3/8" is attached to the center of a standard reference plasma tube, allowing an aluminum test sphere of 3/8" diameter to slide in and out of the plasma and the cavity. A movable iron slug is located in the long quartz tube and attached to the test sphere by a thin nylon filament of such length that the test sphere could be located either in the center of the plasma or outside the cavity. The test sphere is moved and held in either position by a magnet operating the iron slug.

The measurement procedure uses the discharge operating in the pulsed condition as described in Appendix D. All cavity measurements are done in the afterglow. The test sphere is first positioned outside the cavity, and the frequency shift of the TM_{010} mode, due to the plasma presence, is measured as a function of time in the afterglow. The corresponding inferred electron density n_o at the center of the plasma, derived from the frequency shift by the perturbation theory outlined in Appendix A, is shown as curve A of figure E-2. Next, the frequency shift due to the insertion of the test sphere into the center of the plasma is measured as a function of the time in the afterglow. The latter measurements are shown in curve C of figure E-2. The electron density is also measured during the discharge pulse and the early afterglow by a 35 GHz microwave interferometer. These measurements are shown by curve B.

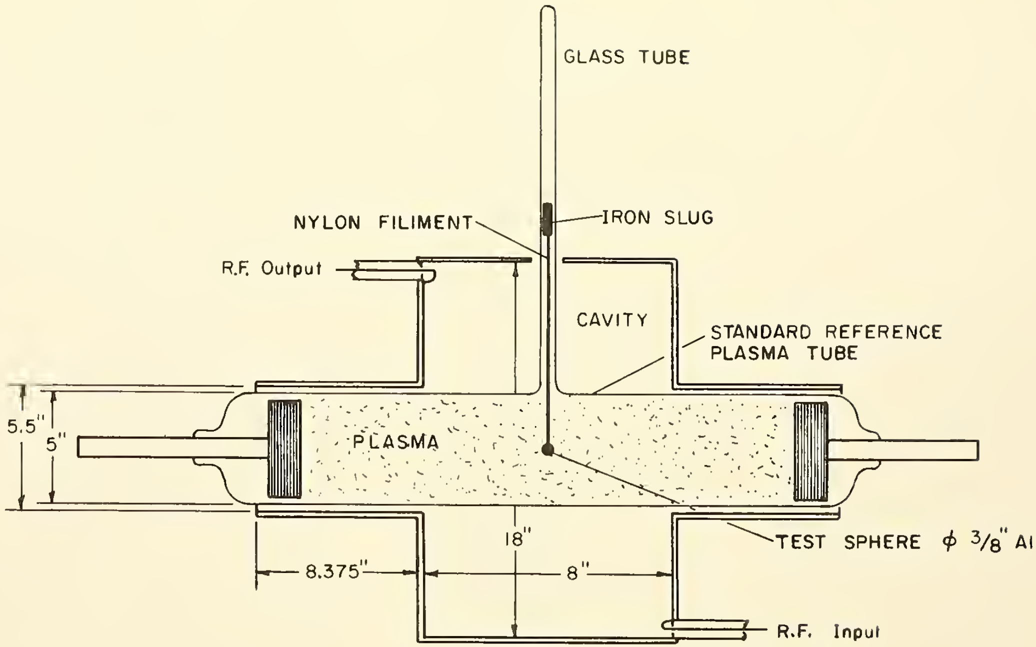

Figure E-1. EXPERIMENTAL ARRANGEMENT OF THE DOUBLE PERTURBATION METHOD.

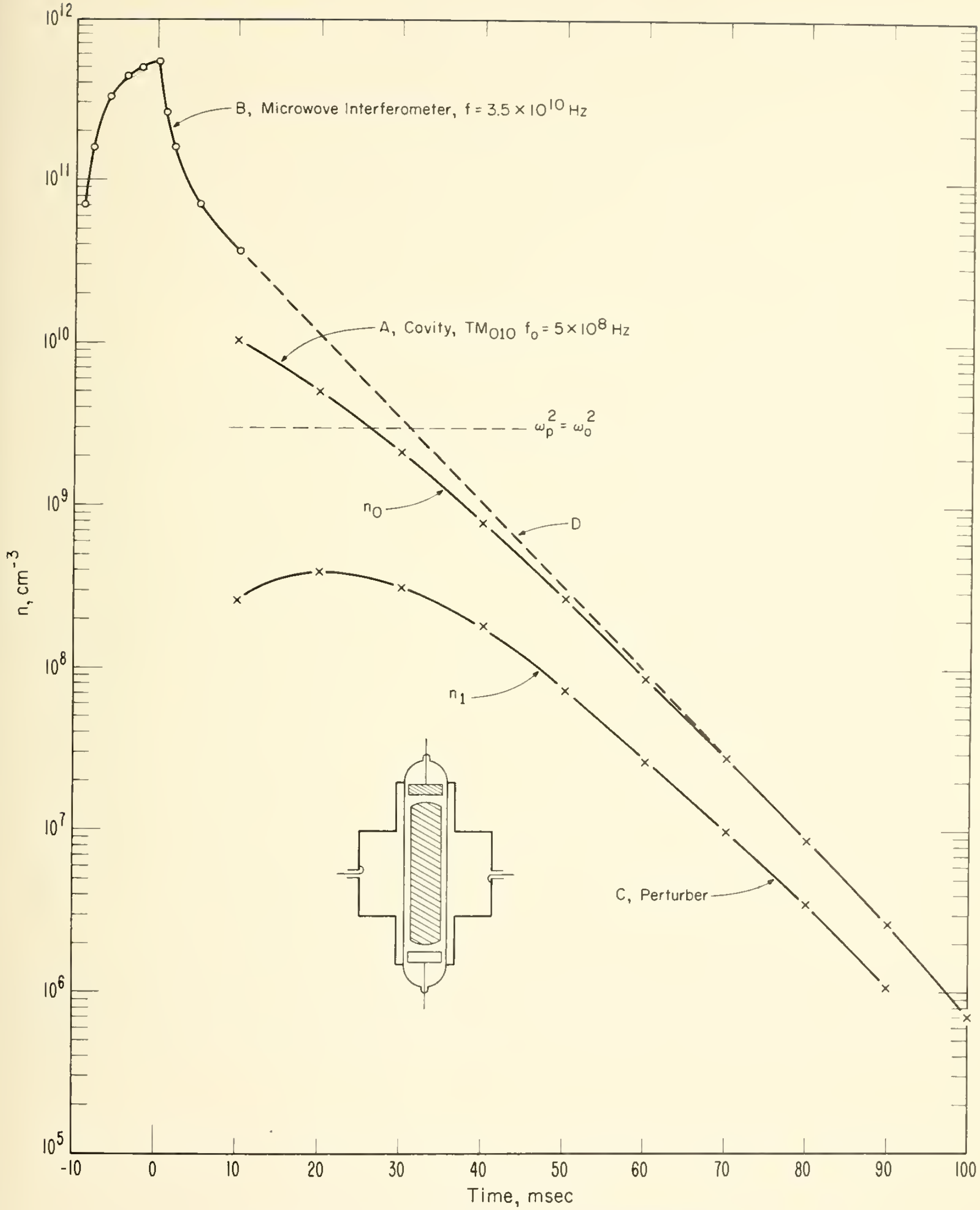

Figure E-2. POLARIZATION MEASUREMENTS

The frequency of the microwave interferometer is large compared to the plasma frequency and the simple perturbation theory applicable for the interpretation of the corresponding measurements. This is also true for the cavity measurements in the late afterglow. The dashed curve D which connects the interferometer measurements with the cavity measurements is, therefore, likely to represent the correct electron density in the range where the cavity measurements are questionable. The two curves are connected by a straight line because in this range the diffusion losses dominate. The ratio between the electron densities for the two curves A and C at any given time in the afterglow are given by curve C in figure E-3. This ratio is considerably less than unity in the early afterglow where the plasma frequency is comparable to or larger than the resonance frequency of the TM_{010} mode, and where one can expect strong polarization effects. This is confirmed by the test sphere measurements.

The density, n_1, derived from the frequency shift due to the insertion of the test sphere into the plasma center is written as

$$n_1 = C\, n_o\, E_p^2, \tag{10}$$

where n_o is the electron density, E_p is the local unperturbed electric field, and C is an undetermined constant. The ratio n_1/n_o is therefore a measure of the electric field E_p at the center of the plasma. Curve A in figure E-3 shows how this ratio varies with the time in the afterglow. Since perturbation theory shows that the polarization effects vanishes as the square of the electron density, and E_p simultaneously goes toward E_o, one can normalize this curve so the ratio becomes unity in the very late afterglow. The normalized curve B should represent the square of the ratio E_p/E_o if perturbation theory remained valid over the entire range.

Both curves B and C from figure E-3 show polarization effects. Curve C compares the cavity measurements and the interferometer measurements and curve B compares the cavity measurements with the test sphere measurements. Both curves have been replotted in figure E-4 as function of the electron density in the center of the plasma. The vertical broken line in this figure shows the electron density where the plasma frequency equals the TM_{010} resonance frequency. The two curves correlate in shape but not in magnitude. The test sphere is more sensitive to the polarization effects than is the direct comparison of the cavity measurements and the interferometer measurements. The higher sensitivity of the test sphere measurements is likely due to the electron density depression around the test sphere which causes additional polarization effects. These effects further decrease the electric field in the neighborhood of the test sphere. Since the latter effect acts in series with the polarization at the outside boundaries of the plasma, it is likely that the frequency shift due to the test sphere should be proportional to $(E_p/E_o)^{\alpha}$ with α larger than 2. A comparison of curves B and C suggest that α is near 4.

The error of the cavity measurements due to the polarization effects are shown by curve C in figure E-4. To have an error of less than 10 percent it is necessary for the electron density at the plasma center to be 30 times less than the critical electron density. The critical electron density is defined by equating the plasma frequency to the empty cavity resonance frequency. It must be emphasized that the errors due to polarization effects depend on both the cavity and plasma configurations.

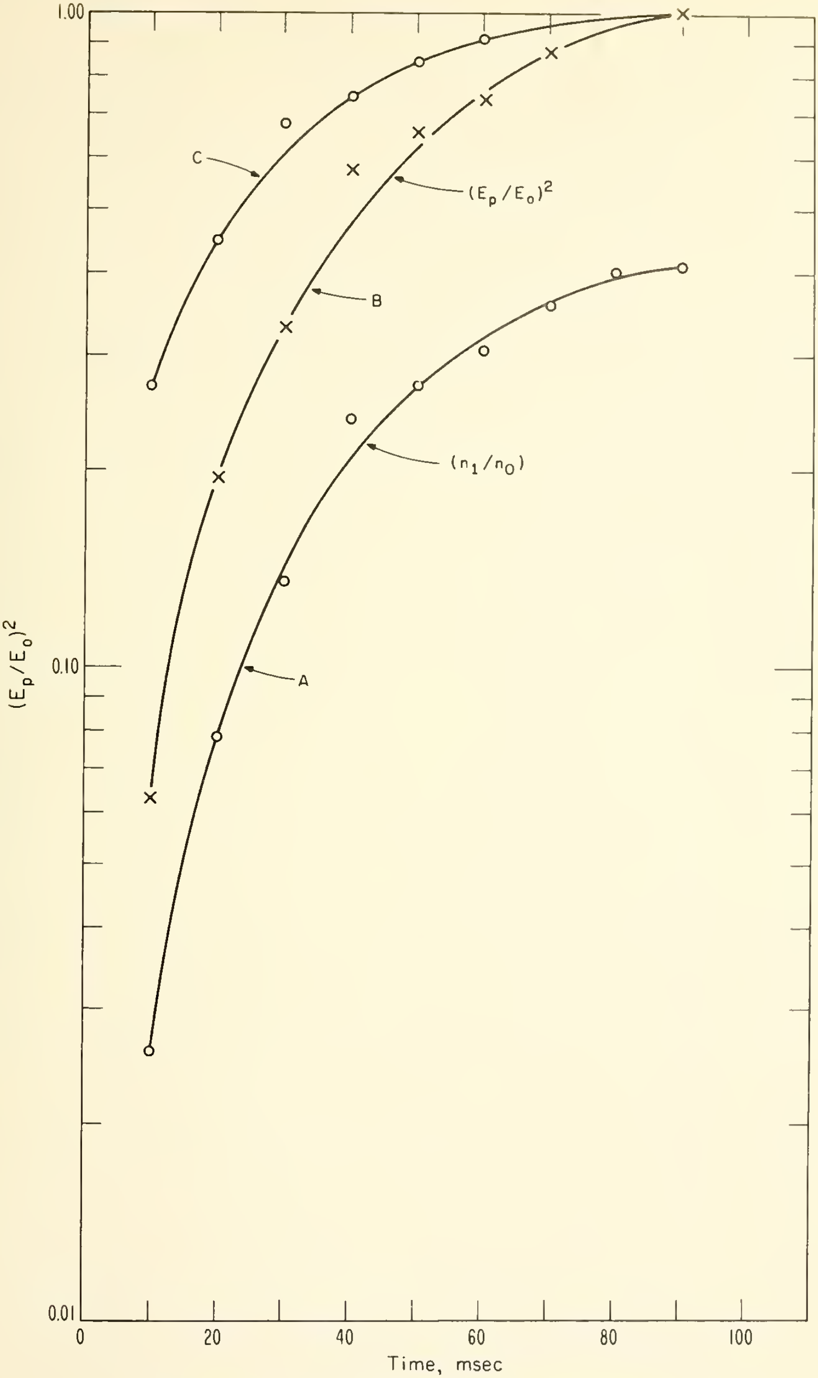

Figure E-3. TEST SPHERE MEASUREMENTS

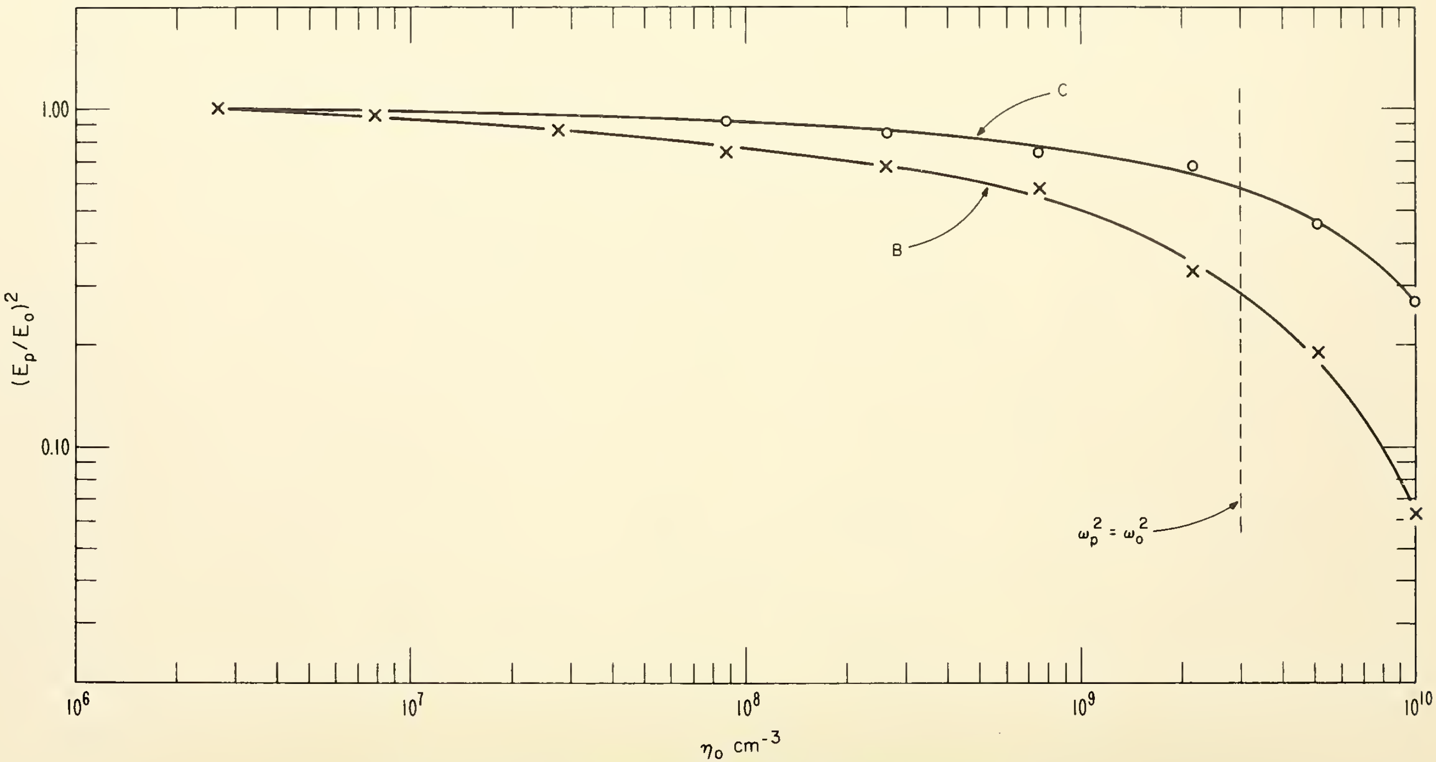

Figure E-4. POLARIZATION VERSUS ELECTRON DENSITY

Appendix F

The frequency shift method

The experimental arrangement for the frequency shift method is shown schematically in figure F-1. The time marker generator C triggers the pulse generator D once every 200 msec. The pulse generated by D controls the current limiting, high voltage pulser E, which, with the help of the high voltage power supply F, generates a current pulse of 50 mA and 10 msec. duration through the standard reference plasma tube, which is inserted in the cavity. The time marker generator C also triggers the scope at the start of the current pulse through the discharge tube. A trigger with a variable time delay, generated by the scope, starts the UHF sweep generator G. The output from this generator is fed through a matched, calibrated, and variable attenuator H followed by an isolator to the input loop of the cavity. The output from the cavity is fed through an isolator and a detector followed by a wide band amplifier I, giving a faithful reproduction of the amplitude envelope of the UHF signal transmitted through the cavity. The pulse corresponding to the UHF amplitude envelope is then fed through an amplitude discriminating amplifier adjusted for peak detection. A fraction of the output from the UHF sweep generator G is also fed into the UHF mixer K where it is mixed with the signal from the UHF signal generator L, which is monitored by the frequency counter M. The Z-axis marker generator N generates a sharp trigger when the frequencies from G and L differ by 450 kHz. This trigger intensifies the spot on the scope at the time when the difference between the two frequencies is 450 kHz. The frequency of the generator L is variable and the bright spot could be located anywhere in time during the scope sweep.

The sweep of the generator is started at time t_1, and its frequency limits are adjusted so that the cavity resonance could be seen between the time t_1 and t_2. The parameters are adjusted so that the trace A coincided with a time marker t_3 as is shown in figure F-2. The frequency of the signal generator L is changed until the bright spot was located at the maximum of the transmitted signal. The reading on the frequency counter then gave the cavity resonance frequency containing the plasma corresponding to the time t_3 in the after glow. The attenuator H is adjusted so that the trace A has a predetermined height on the screen, and the reading on the attenuator is recorded. This process is repeated at regular intervals in the afterglow, from the early afterglow with very high electron densities, to the very late after glow where the plasma has disappeared. The measurements in the very late afterglow serve as reference data, defining the empty cavity resonance frequency, ω_o, and the transmission amplitude S_o for the TM_{010} mode.

With the available equipment and the method outlined above, the resonance frequency is easily determined to within one part in 10^5. The transmitted amplitude at resonance had about a 1% error in the absence of noise. It is difficult to measure the peak amplitude of a transient UHF signal when a large dynamic range is required. These difficulties are due to the width variation of the detected UHF envelope induced by the changing Q. Since a large dynamic range requires considerable amplification after the detection, the amplitude becomes sensitive to the frequency characteristics of the amplifiers, which must be narrow banded to reduce noise. The amplitude discrimination by the amplifier, J, solves this problem. About 5 per cent of the peak of the detected UHF signal envelope is amplified and used as a null signal by adjusting the attenuator H so that the height of that null signal, as observed on the screen, is always the same.

To insure that the cavity measurements relate correctly to the electron density and the electron collision frequency, it is necessary to demonstrate that the measured quantities are reasonably independent of changes in the measurement system. The loop couplings to the cavity, and the amplifier with amplitude discrimination are the most critical parts of the measurements system; therefore measurements were made with different size loops located in different parts of the cavity. In each configuration, measurements were done with the amplitude discrimination on and off. Two different loop sizes were used; a standard loop with a loop area of 1.5 cm^2 and a larger loop with a loop area of 20 cm^2. A representative set of measurements with

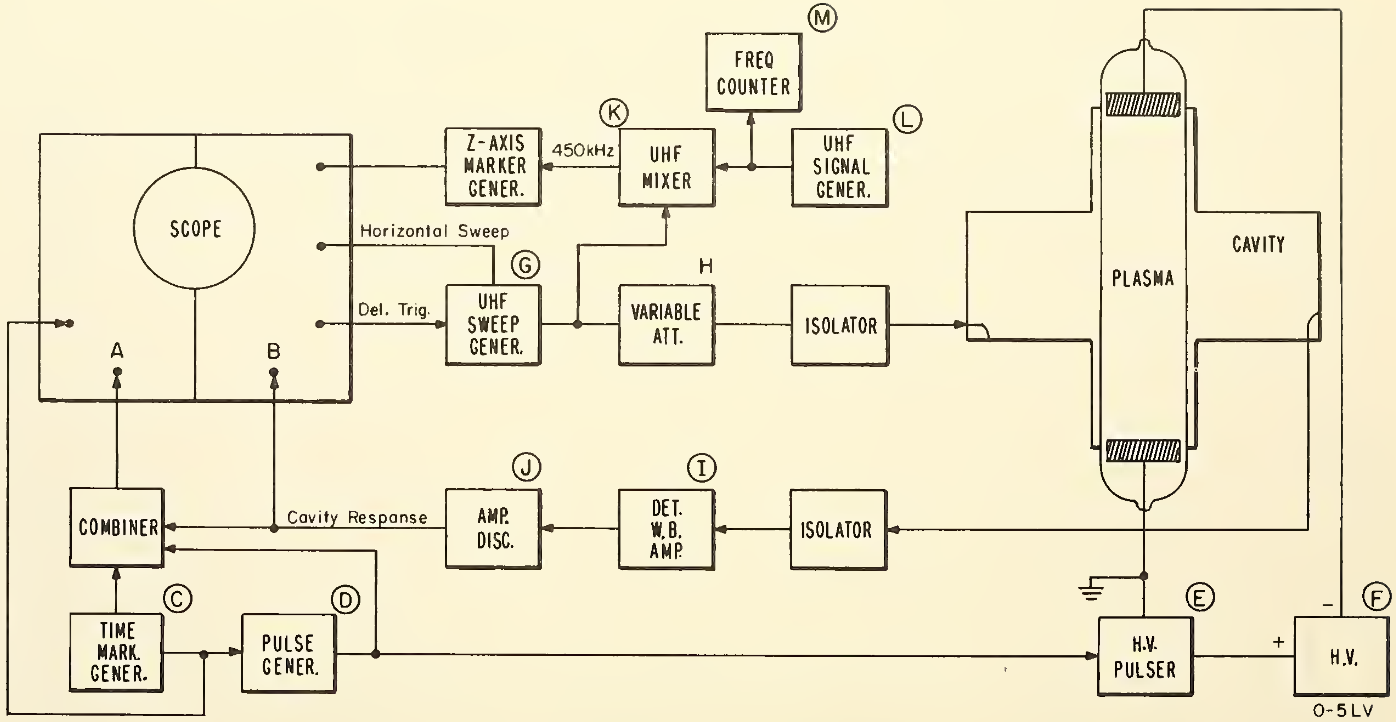

Figure F-1. BLOCK DIAGRAM OF CIRCUIT

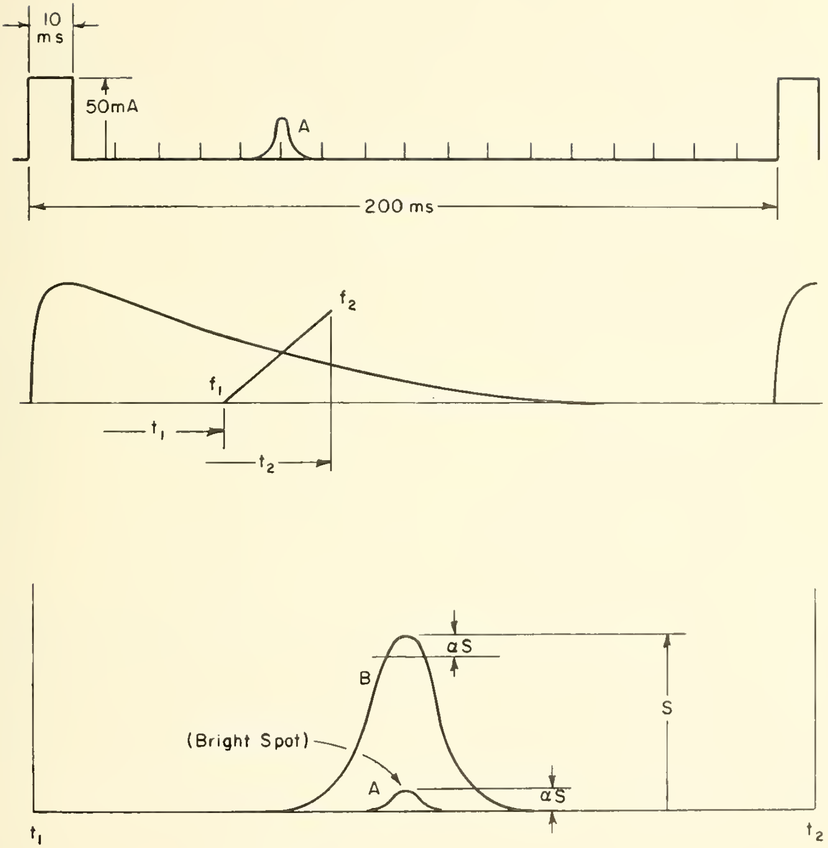

Figure F-2. OSCILLOSCOPE DISPLAYS

amplitude discrimination effective, are shown in figure F-3. In this figure is plotted

$$\frac{\omega_1 - \omega_o}{\omega_o} \tag{1}$$

and the quantity

$$\frac{1}{2Q_L}\left(\frac{S_o'}{S_p'} - 1\right) \tag{2}$$

versus the time in the afterglow. The corresponding measurements with the amplitude discrimination ineffective are shown in figure F-4. We see that the relative frequency shift of the cavity-plasma system is fairly independent of the loop size, and of the amplitude discrimination. The coupling and the electronics have however definite influence on the losses as represented by (2). However, it is more informative to discuss the coupling and electronic influence in terms of the loss factor

$$\frac{\nu_m}{\omega} = \frac{\frac{1}{2Q_L}\left(\frac{S_o'}{S_p'} - 1\right)}{\frac{\omega_r - \omega_o}{\omega_o}} \tag{3}$$

where all quantities on the right are obtained from our measurements. This loss factor is, according to the perturbation theory, independent of the electron density, if the degree of ionization is such that the electron-ion interaction can be neglected.

The average electron momentum transfer collision frequency ν_m is defined [15] as

$$\nu_m = n_g \frac{\int Q_m(v)\, v\, v\, f(v)\, d^3v}{\int v\, f(v)\, d^3v} \tag{4}$$

where Q_m is the momentum transfer collision cross section and $f(v)$ the electron velocity distribution. The momentum transfer collision cross section for the interaction between electrons and helium atoms is essentially independent of the electron energy at energies less than 1 eV. This cross section can therefore be considered as a constant for the abnormal negative glow in helium and its afterglow. The electron velocity distribution of the abnormal negative glow and its afterglow can, for all practical purposes, be assumed to be Maxwellian. Introducing a Maxwellian velocity distribution function, slightly perturbed by the measuring field, it is easily shown that formula (4) reduces to

$$\nu_m = n_g Q_m \frac{8}{\sqrt{3\pi}} \sqrt{\frac{2kT}{m}} \;. \tag{5}$$

At a pressure of 1 Torr and room temperature, one finds, by introducing the latest [16] momentum transfer collision cross section, 5.2×10^{-16} cm^2, measured in electron beam experiments, that $\nu_m = 2.6 \times 10^8$ sec^{-1} giving a loss factor of

$$\nu_m/\omega = 8.3 \times 10^{-2} \tag{6}$$

at the frequency 5×10^8 Hz used in the present measurements. The loss factor is proportional to the square root of the electron temperature, but since this temperature essentially is constant at times after 10 msec. in the afterglow and since the electron-ion interaction can be neglected at times later than 10 msec., it follows that the loss factor obtained in bona fide measurements should be constant, independent of the time, for measurements done later than 10 msec. in the afterglow.

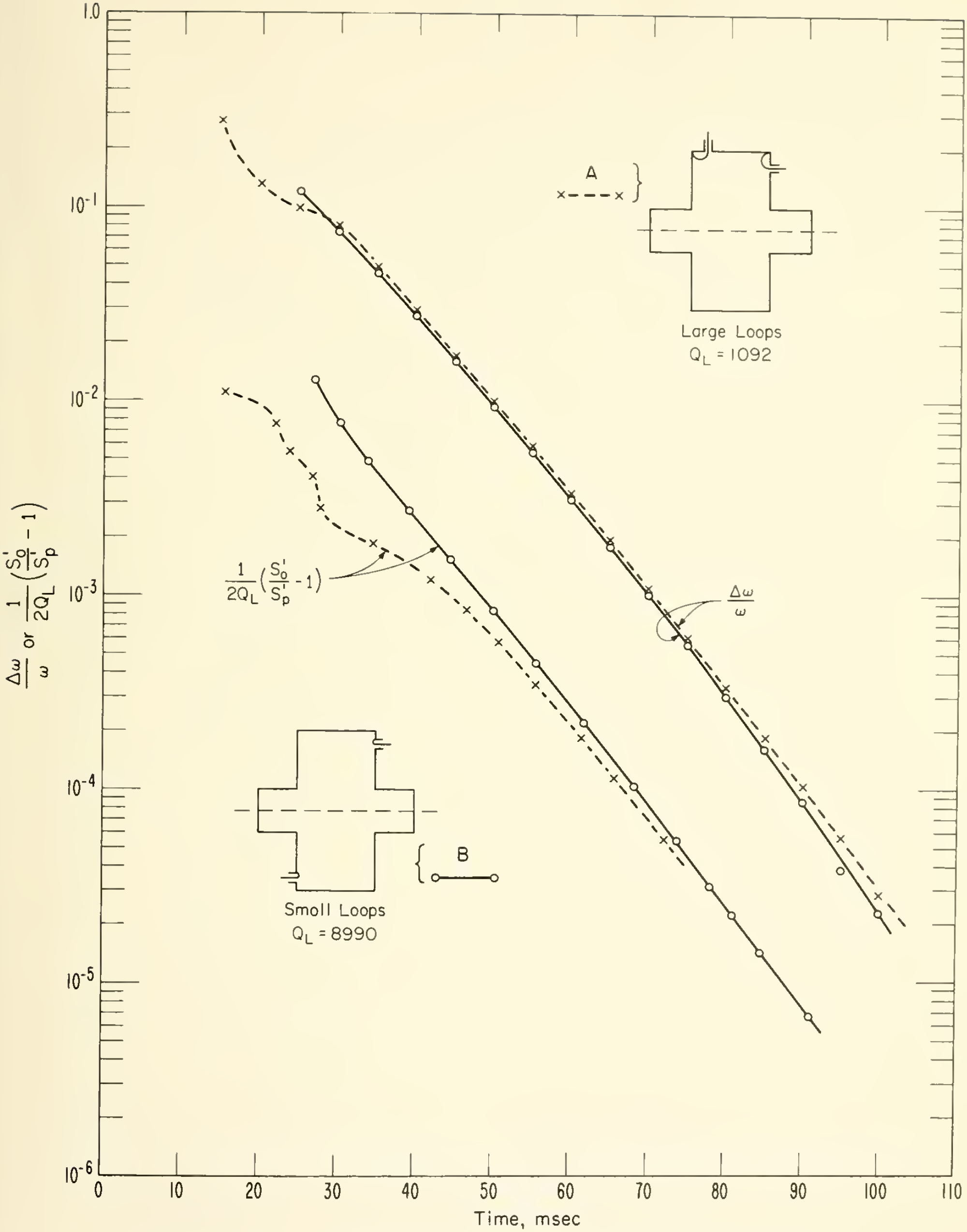

Figure F-3. MEASUREMENTS WITH AMPLITUDE DISCRIMINATION

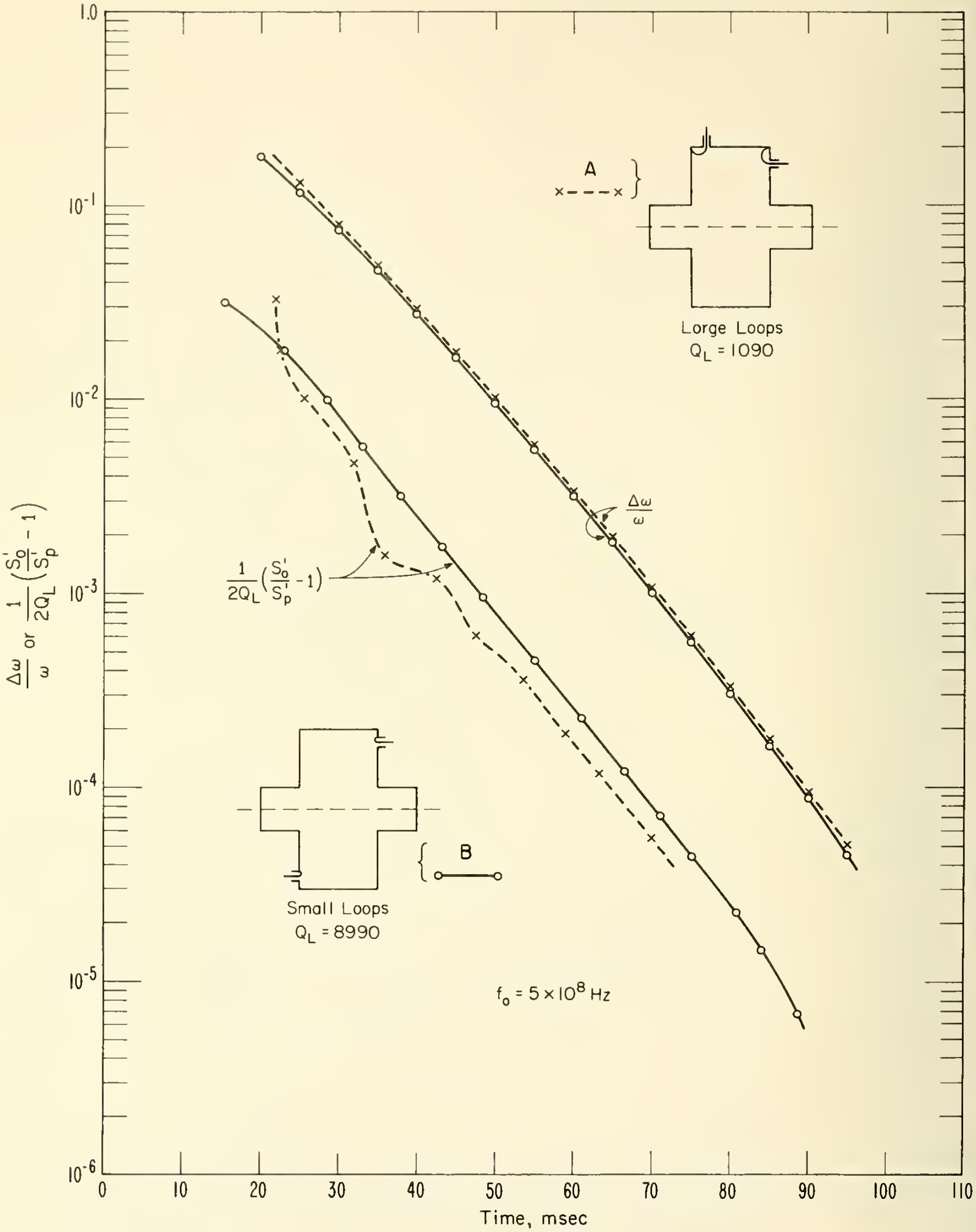

Figure F-4. MEASUREMENTS WITHOUT AMPLITUDE DISCRIMINATION

The loss factors obtained from the measurements shown in figures F-3 and F-4 have been plotted in figure F-5 as function of the time in the afterglow and the corresponding electron density. The fully drawn curves represent the data taken with the amplitude discrimination effective, while the broken lines represent the data obtained with the amplitude discrimination turned off. The two curves giving the largest loss factors were obtained with the small loop and the two curves giving the smallest loss factors were obtained with the large loops. The horizontal, fully drawn line represents the constant loss factor derived from the most recent electron beam scattering experiments. One observes that the loss factors are not independent of the time in the afterglow and that obviously the loop size and location as well as the amplitude discrimination have considerable influence on the measurements. Only one measurement set gives a loss factor which agrees with the value obtained from the beam experiments, and then only when the electron density is less than 10^8 cm^{-3}. That data is obtained by using the small loops and amplitude discrimination.

The scatter in the data as shown in figure F-5 indicates that the differences between the curves must be viewed as systematic errors. These systematic errors have the following sources:

1. The generation, due to the onset of polarization of the plasma with increasing electron density, of irrotational and solenoidal modes.

2. The generation of higher solenoidal modes, due to the finite size of the loops, which interact differently with the plasma than the TM_{010} mode does.

3. Systematic errors in the amplitude measurements due to the transient UHF signals.

The first type of systematic error is evident in the curves B, figure F-5, which were obtained with the small loops. The loss factor increases with increasing electron density. A comparison to the polarization measurement as discussed in Appendix E shows that the increase in the loss factor becomes evident when the polarization effects show up.

The second type of systematic error is demonstrated by curves A, figure F-5. The loops are now so large and the loaded Q of the cavity system so low, that there is significant coupling between the loops by modes other than the TM_{010} mode. This situation is described by saying that the signal can be split up into two parts; one part which does interact with the plasma and another part which does not. Whether these signals add or subtract depends on their relative phase relationship. This phase depends on the loop sizes, their locations and orientation as well as on the plasma and loaded Q. This accounts for the radically different behavior of the curves A and B as function of the time in the afterglow or as function of the electron density.

The first type of systematic error manifests itself in the measurements of the average electron density $\langle n \rangle_{aa}$, the filling factor, and the loss factor ν_m/ω. They are characteristic of the cavity, the mode used for the measurements, and the plasma configuration. These errors are inherent to the present cavity system. Appendix A shows that these errors happen when the plasma approaches the dense condition. The measurements discussed here and in Appendix E show errors which are noticeable at electron densities considerably smaller than the critical electron density. The critical electron density for the cavity used is 3.1×10^9 cm^{-3}. We see from Figures F-5 and E-4 that errors due to the polarization effects become noticeable at electron densities less than 10^8 cm^{-3}.

The second and third class of systematic errors can be eliminated. The second class of errors is primarily related to the design of the couplings to the cavity; the size of the loops, their orientation and location. The third class depends on the design of the electronics used for measuring the relative amplitude of the signal. It is important to notice that the average electron density as measured by the frequency shift method

$$\frac{\langle n \rangle_{aa}}{1+\left(\frac{\nu_m}{\omega}\right)^2} = \frac{2m\varepsilon_o \omega^2}{e^2} \frac{\Delta\omega}{\omega} \qquad (7)$$

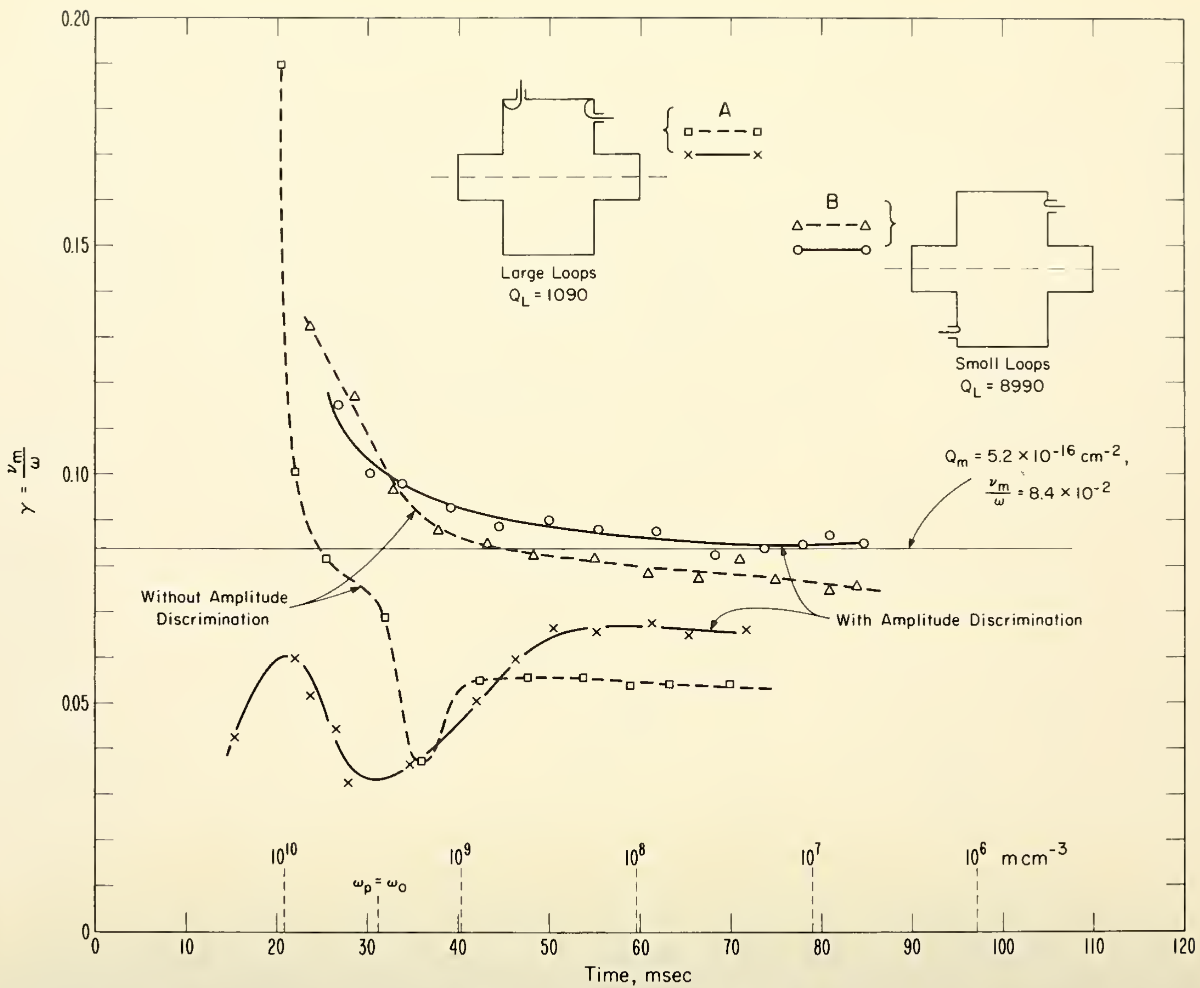

Figure F-5. LOSS FACTOR MEASUREMENTS

which in this case, for all practical purposes, is equal to the average electron density $\langle n \rangle_{aa}$, is not influenced by systematic errors belonging to the second and third classes, provided it is measured with the frequency shift method. This is predicted by theory and confirmed experimentally by the data shown in figures F-3 and F-4. When the same quantity is measured with the amplitude and phase shift method, it is written as

$$\frac{\langle n \rangle_{aa}}{1 + \left(\frac{\nu_m}{\omega}\right)^2} = \frac{m \varepsilon_o \omega^2}{e^2} \frac{1}{Q_L} \frac{S_o}{S_p} \operatorname{Sin} (\varphi_p - \varphi_o) \quad . \qquad (8)$$

and is now subject, not only to the systematic errors associated with the polarization effects, but also to all systematic errors belonging to the second and third classes as well as to a new group of errors associated measuring the relative phase of a transient UHF signal.

The frequency shift method discriminates very well against undesirable modes, a quality entirely missing in the amplitude and phase shift method. This is explained by figure F-6 where a frequency swept signal transmitted through the cavity has been plotted as function of the frequency. The curve A represents the amplitude of the mode assumed to be used for the measurements and has the resonance frequency f_p in the presence of the plasma. The curve B is the amplitude of an undesirable mode with the resonance frequency f'_p while f_o is the resonance frequency of the mode A in the absence of the plasma. The broken curve represents the total signal due to both modes. The frequency shift method measures the frequency at which the transmitted signal amplitude has a maximum. It is obvious from figure F-6 that the determination of the resonance frequency of the mode A is relatively insensitive to the presence of the mode B, in particular if the Q of the system is relatively high. The amplitude and phase shift method does all the measurements at the frequency f_o. It cannot decide whether an undesirable signal is present and measures the sum, with the appropriate phase relation, of the signal associated with both modes.

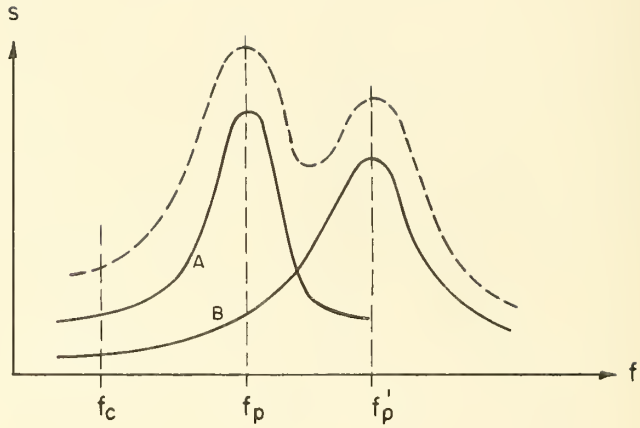

Figure F-6. MODE MIXING

FORM NBS-114A (1-71)

<table>
<tr><td>U.S. DEPT. OF COMM.
BIBLIOGRAPHIC DATA SHEET</td><td>1. PUBLICATION OR REPORT NO.
NBS-TN-607</td><td>2. Gov't Accession No.</td><td>3. Recipient's Accession No.</td></tr>
<tr><td colspan="3" rowspan="2">4. TITLE AND SUBTITLE
"The Errors in Plasma Measurements by the Microwave Cavity Techniques"</td><td>5. Publication Date
October 1971</td></tr>
<tr><td>6. Performing Organization Code</td></tr>
<tr><td colspan="3">7. AUTHOR(S)
K-B Persson and E. G. Johnson, Jr.</td><td>8. Performing Organization</td></tr>
<tr><td colspan="3" rowspan="2">9. PERFORMING ORGANIZATION NAME AND ADDRESS
NATIONAL BUREAU OF STANDARDS, Boulder Labs
DEPARTMENT OF COMMERCE
Boulder, Colorado 80302</td><td>10. Project/Task/Work Unit No.
2710161</td></tr>
<tr><td>11. Contract/Grant No.
NR 012-111</td></tr>
<tr><td colspan="3" rowspan="2">12. Sponsoring Organization Name and Address
Advanced Research Projects Agency
1400 Wilson Blvd.
Arlington, Virginia 22209</td><td>13. Type of Report & Period Covered</td></tr>
<tr><td>14. Sponsoring Agency Code</td></tr>
<tr><td colspan="4">15. SUPPLEMENTARY NOTES</td></tr>
</table>

16. ABSTRACT (A 200-word or less factual summary of most significant information. If document includes a significant bibliography or literature survey, mention it here.)

This report presents the results of a theoretical and experimental study of the microwave cavity techniques used in measuring electron density and collision frequency in transient plasmas. Sources of errors are discussed and certain calibration procedures are recommended to minimize the error. In particular, the abnormal negative glow discharge in helium is presented as an inexpensive reference plasma for calibration purposes.

17. KEY WORDS (Alphabetical order, separated by semicolons)

Collision frequency; helium negative glow discharge; microwave cavity; plasma density.

<table>
<tr><td rowspan="2">18. AVAILABILITY STATEMENT

[x] UNLIMITED.

[ ] FOR OFFICIAL DISTRIBUTION. DO NOT RELEASE TO NTIS.</td><td>19. SECURITY CLASS (THIS REPORT)
UNCLASSIFIED</td><td>21. NO. OF PAGES
64</td></tr>
<tr><td>20. SECURITY CLASS (THIS PAGE)
UNCLASSIFIED</td><td>22. Price
65 cents</td></tr>
</table>

NBS TECHNICAL PUBLICATIONS

PERIODICALS

JOURNAL OF RESEARCH reports National Bureau of Standards research and development in physics, mathematics, chemistry, and engineering. Comprehensive scientific papers give complete details of the work, including laboratory data, experimental procedures, and theoretical and mathematical analyses. Illustrated with photographs, drawings, and charts.

Published in three sections, available separately:

- **Physics and Chemistry**

Papers of interest primarily to scientists working in these fields. This section covers a broad range of physical and chemical research, with major emphasis on standards of physical measurement, fundamental constants, and properties of matter. Issued six times a year. Annual subscription: Domestic, $9.50; $2.25 additional for foreign mailing.

- **Mathematical Sciences**

Studies and compilations designed mainly for the mathematician and theoretical physicist. Topics in mathematical statistics, theory of experiment design, numerical analysis, theoretical physics and chemisty, logical design and programming of computers and computer systems. Short numerical tables. Issued quarterly. Annual subscription: Domestic, $5.00; $1.25 additional for foreign mailing.

- **Engineering and Instrumentation**

Reporting results of interest chiefly to the engineer and the applied scientist. This section includes many of the new developments in instrumentation resulting from the Bureau's work in physical measurement, data processing, and development of test methods. It will also cover some of the work in acoustics, applied mechanics, building research, and cryogenic engineering. Issued quarterly. Annual subscription: Domestic, $5.00; $1.25 additional for foreign mailing.

TECHNICAL NEWS BULLETIN

The best single source of information concerning the Bureau's research, developmental, cooperative, and publication activities, this monthly publication is designed for the industry-oriented individual whose daily work involves intimate contact with science and technology—*for engineers, chemists, physicists, research managers, product-development managers, and company executives.* Annual subscription: Domestic, $3.00; $1.00 additional for foreign mailing.

NONPERIODICALS

Applied Mathematics Series. Mathematical tables, manuals, and studies.

Building Science Series. Research results, test methods, and performance criteria of building materials, components, systems, and structures.

Handbooks. Recommended codes of engineering and industrial practice (including safety codes) developed in cooperation with interested industries, professional organizations, and regulatory bodies.

Special Publications. Proceedings of NBS conferences, bibliographies, annual reports, wall charts, pamphlets, etc.

Monographs. Major contributions to the technical literature on various subjects related to the Bureau's scientific and technical activities.

National Standard Reference Data Series. NSRDS provides quantitative data on the physical and chemical properties of materials, compiled from the world's literature and critically evaluated.

Product Standards. Provide requirements for sizes, types, quality, and methods for testing various industrial products. These standards are developed cooperatively with interested Government and industry groups and provide the basis for common understanding of product characteristics for both buyers and sellers. Their use is voluntary.

Technical Notes. This series consists of communications and reports (covering both other agency and NBS-sponsored work) of limited or transitory interest.

Federal Information Processing Standards Publications. This series is the official publication within the Federal Government for information on standards adopted and promulgated under the Public Law 89–306, and Bureau of the Budget Circular A–86 entitled, Standardization of Data Elements and Codes in Data Systems.

Consumer Information Series. Practical information, based on NBS research and experience, covering areas of interest to the consumer. Easily understandable language and illustrations provide useful background knowledge for shopping in today's technological marketplace.

NBS Special Publication 305, Supplement 1, Publications of the NBS, 1968-1969. When ordering, include Catalog No. C13.10:305. Price $4.50; $1.25 additional for foreign mailing.

Order NBS publications from: Superintendent of Documents
Government Printing Office
Washington, D.C. 20402

U.S. DEPARTMENT OF COMMERCE
National Bureau of Standards
Washington, D.C. 20234

OFFICIAL BUSINESS

Penalty for Private Use, $300

POSTAGE AND FEES PAID
U.S. DEPARTMENT OF COMMERCE

U.S.MAIL